Synthesis of Ceria Nanomaterials to Enhance Catalytic Activity of CO Oxidation

by

Myeongseok Sim

A thesis submitted to the Graduate Faculty of
Auburn University
in partial fulfillment of the
requirements for the Degree of
Master of Science

Auburn, Alabama
December 14, 2019

Keywords: Catalysis, Electrospinning, CO oxidation, Composite materials, Ceria nanofibers

Approved by

Tae-Sik Oh, Chair, Assistant Professor of Chemical Engineering
Maria Auad, W. Allen and Martha Reed Professor of Chemical Engineering
Carlos Carrero, Assistant Professor of Chemical Engineering

Abstract

This thesis represents a comparative study of a series of ceria nanomaterials towards CO oxidation. Ceria particles were synthesized using microwave-assisted hydrothermal and one-step solvothermal methods, and ceria nanofibers were synthesized using the electrospinning technique. 6 transition metals have been selected namely, copper (Cu), nickel (Ni), cobalt (Co), manganese (Mn), iron (Fe), and lanthanum (La) as dopants for ceria nanofibers. The formation and respective physicochemical properties of the materials were confirmed by employing XRD analysis, BET surface area measurements, SEM, TEM, Raman, and XPS techniques. All the doped ceria nanofibers exhibited smaller crystallite size and higher amounts of oxygen vacancies than that of pure ceria. CO oxidation was performed in the presence of oxygen under atmospheric pressure and 300-750K temperature range in a fixed bed reactor. The physicochemical properties of the ceria materials were comparatively analyzed to correlate the influence of dopants with their CO oxidation activity. The role of 'lattice oxygen' and surface areas was considered, assuming that Mars Van Krevelen (MVK) mechanism plays a key role in CO oxidation activity. For the pure ceria materials with different morphologies, they had similar CO oxidation activity when they have similar BET surface area values. Copper doping significantly increased the CO oxidation activity and the already existing oxygen vacancy was not the determining factor for the CO oxidation.

Acknowledgments

I would like to give special thanks to my advisor Dr. Tae-Sik Oh. I was not good enough, and I would not be able to finish my master's degree without his advising. I believe he will accomplish a lot in our department as an engineer.

Also, I would like to thank my committee members, Dr. Maria Auad and Carlos Carrero. They were always kind and opened to questions regarding my research.

Also, I hope my lab members finish their degrees with big achievements. They assisted me a lot and I was able to do experiments safely with their help.

Lastly, I would like to appreciate my lovely family. My parents always trust me and give me big helps whenever I need them. My hardworking sister and brother-in-law always give me courage even without saying anything.

Table of Contents

List of Tables

List of Figures

Chapter 1

INTRODUCTION

Synthesizing ceria materials has drawn extremely large research interest because of their considerable use in environmental, energy-related catalytic applications. Ceria gained a lot of attention because of its redox catalytic property and oxygen storage capacity (OSC) [1]. The easy transition between Ce^{4+} and Ce^{3+} oxidation states and the formation of internal oxygen vacancies give superior redox property in ceria [2]. Furthermore, nanoscale ceria displays significant catalytic activity compared to bulk ceria and that is because of an increased specific surface area and easier oxygen vacancy formation [3]. However, pure ceria has limitations to be used for commercial applications. Deactivation of the redox couple, low OSC, reduction of catalytic activity and significant loss of active area by thermal sintering are few among them. Even a small extent of sintering causes a magnificent effect on the crystallite size and oxygen vacancies that leads to lowering the catalytic effect [4]. However, adding foreign metal ions in the ceria lattice is well known to strengthen itself against loss of catalytic activity and thermal sintering [5]. The choice of appropriate dopants is still a big challenge in terms of thermal stability, oxygen storage and price. Researchers have been studied to correlate the effects of dopant features such as ionic radius, electronegativity, oxidation state, etc.

Among techniques synthesizing nanomaterials, electrospinning is a widely used technique utilizing electrical forces to synthesize polymer fibers using polymer solutions of both synthetic and natural polymers. This technique provides a means for synthesizing nanofibers with various pore structures [6]. Also, it gained a lot of attention for the last decade due to its capability of consistently synthesizing fibers in the nanoscale range and spinning a wide range of polymeric fibers that is difficult to produce using conventional mechanical fiber-spinning techniques [7].

Electrospun nanofibers give advantages such as high surface-to-volume ratio, adjustable porosity, malleability to tailored to a variety of shapes and sizes and capability to control its composition to attain the desired results based on the properties. With these advantages, electrospun nanofibers were used for various applications such as sensors, filtration, biological scaffolds and electrode materials [8].

Carbon monoxide (CO) is a colorless, toxic and tasteless gas. A human can even die if they are exposed to CO gas for a certain time. CO oxidation has been given a lot of attention since it plays a substantial role in CO gas sensors, indoor air cleaning, CO_2 lasers and automotive exhaust treatment [9]. There were a lot of efforts to efficiently increase the catalytic activity of CO oxidation using low-cost materials and researchers are working on the development of materials to effectively remove CO.

In this study, ceria particles were synthesized using two different methods and ceria-based electrospun nanofibers were synthesized using the electrospinning technique to measure catalytic activities of CO oxidation. To study the effects of dopants, transition metals (Cu, Mn, Fe, Co, Ni, and La) were used and each dopant was mixed in 10 and 30 mol% concentration. For comparison, undoped ceria nanofibers were synthesized under equal conditions. The synthesized materials were characterized by means of various techniques, X-ray diffraction (XRD), Raman spectroscopy (RS), Brunauer-Emmett-Teller (BET) surface area, X-ray photoelectron spectroscopy (XPS), transmission electron microscopy (TEM) and scanning electron microscope (SEM). The catalytic activity was investigated towards the oxidation of CO in a fixed bed reactor and attempts were made to correlate the CO oxidation activity results with the characterization studies.

Chapter 2

BACKGROUND INFORMATION

Ceria Properties and Applications

2. 1. 1 Ceria (CeO_2)

Ceria-based oxides have attained an important position as active advanced materials and co-catalysts for energy conversion systems and environmental applications. Every year since 2006, over a thousand publications related to ceria are printed, and it demonstrates the enormous scientific interest. It is reported that the irreplaceable role of ceria for car exhaust gas pollution control, and it has a promising future in many sectors such as catalysts, fuel cells, and photocatalysts. Also, it is the most abundant among the rare-earth elements, and it is more abundant than nickel or copper.

2. 1. 2 Electronic Structure

Ceria is the most stable oxide form of cerium oxides. Cerium is the most reactive among lanthanide elements and it is electropositive in nature. Cerium exists in dual oxidation states, Ce^{4+} and Ce^{3+}. The Ce^{4+} oxidation state is considered more stable than Ce^{3+} because its electronic structure is more stable (Ce^{4+} is $[Xe]4f^0$ and Ce^{3+} is $[Xe]4f^1$). Cerium usually exists with two oxides named cerium dioxide (CeO_2) and cerium sesquioxide (Ce_2O_3), but generally, cerium oxide is considered as CeO_2 because of higher stability over Ce_2O_3.

2. 1. 3 Crystal Structure of Ceria

Ceria has a fluorite structure (FCC) with an Fm3m space group. As figure 1 shows, ceria consists of a simple cubic oxygen sub-lattice with cerium ions occupying the cube centers. Figure 1

shows the structure of the ceria with the eight coordinated cerium and the four coordinated oxygen. Cerium is at the center of tetrahedron with corners filled with oxygen atoms [10]. The cubic unit cell's lattice constant is 0.541 nm. The O anions are bonded to four Ce neighbors and Ce cations are bonded to eight O neighbors.

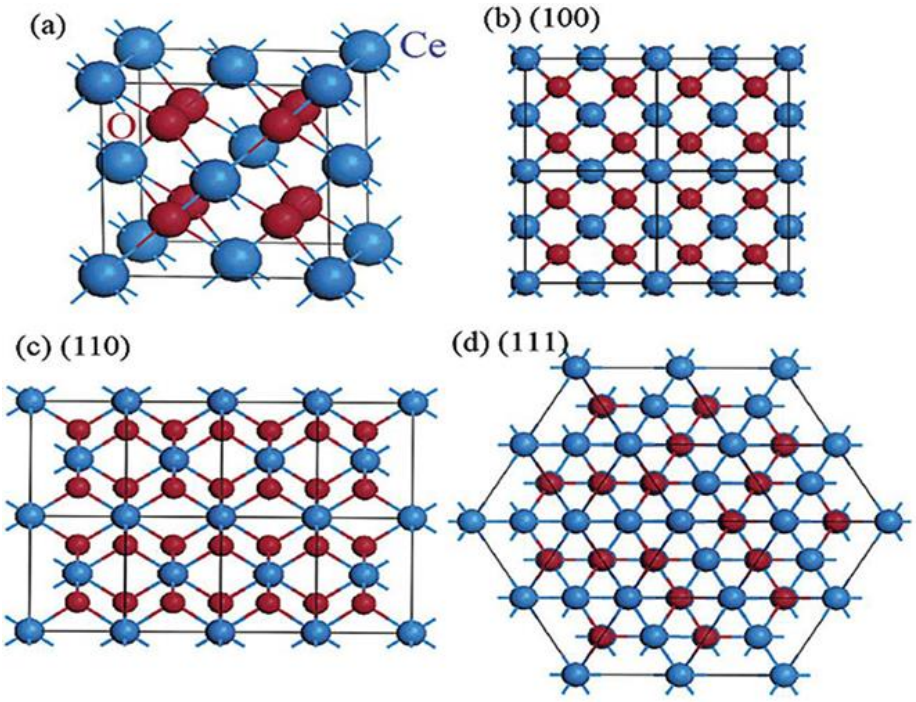

Figure 1. (a) Face-centered crystal cell of the ceria structure. (b-d) The (100), (110) and (111) planes of the ceria structure [11].

2. 1. 4 Defect Chemistry in Bulk Ceria

Ideally, for a crystalline solid, atoms are periodically arranged symmetrically. The composition of a crystal structure is based on a combination of an infinite space lattice, and the space lattice consists of unit cells and the combination of unit cells forms the whole crystalline structure. Imperfections are occurred in crystal structures because of displacements of atoms from their lattice positions, and it leads to breaking the symmetry of the periodic crystalline lattice. In ceria,

intrinsic and extrinsic defects can occur. The occurrence of an intrinsic defect can be because of thermal disorderliness in crystal, which can be occurred due to redox reactions between the solid and atmosphere. But Frenkel and Schottky defects are more probable crystalline intrinsic defects. The extrinsic defects are generally formed by adding impurities or foreign dopants.

2. 1. 5 Oxygen Vacancies in Ceria

Cerium oxide can contain high oxygen deficiency by substituting lower valent elements from the cation sub-lattice. Because of this property, high oxygen ion conductivities are anticipated, which implies its potential applications as a solid electrolyte. Also, ceria is well known for giving off a significant amount of oxygen at low oxygen partial pressure. Due to its ease in redox-based reactions, ceria can have several oxidation states such as Ce^{4+} and Ce^{3+}. Therefore, electrons in ceria can be considered to exist as small polarons. Also, for transport and carrier properties, the concentration of the oxygen vacancies can play a role in oxygen-ion transport in the solid [12]. Three index lattice planes ((100), (110) and (111)) exist on the surface of ceria nanocrystals. The stability order of the planes is (111) > (110) > (100) and the activity is in the reverse order [11]. The oxygen vacancies' formation energy of (111) facet is greater than (100) and (110) facets. Therefore, more oxygen vacancies exist on the (100) and (110) facets than (111) facet. For instance, ceria nanoparticles generally comprise octahedral shapes and mainly most stable (111) facets are exposed in order to keep surface energy as small as possible. Nanocubes and nanorods have more oxygen vacancies on the surfaces because they can expose (100) planes. Meantime, the concentration of oxygen vacancies can be influenced by other external or internal components like doping elements and temperature [13]. The presence of oxygen vacancies in the crystal is a very important phenomenon. The high concentration of

oxygen vacancies makes it easier for the movement of oxygen atoms within the crystal, and that helps redox reactions on its surface for superior catalytic activities.

2. 1. 6 Nano-size Effects of Ceria

By decreasing the material size, ceria nanomaterials show the development of more oxygen vacancies. The high surface area to volume ratio in nanomaterials allows ceria to react differently with unique properties. For example, the higher catalytic activity of CO oxidation was observed by 3-4 nm-sized ceria nanoparticles supporting Au compared to the regular bulk cerium oxide supporting medium [14]. Accordingly, it is possible to control the reactivity of ceria nanoparticles by controlling their size. In addition, nano-sized ceria can have improved size lattice relaxation, electronic conductivity, and other effects compared to bulk ceria.

2. 1. 7 Catalytic Applications of Ceria

The reversible transition between Ce^{4+} and Ce^{3+} makes it possible for the oxygen uptake and release of ceria and this property makes this material as a key ingredient for catalytic reactions and applications. Various ceria structures have been invented, and their catalytic applications are widely reported in recent years. A carbon monoxide oxidation reaction is extensively studied in this category. Ceria nanomaterials can enhance oxygen storage capability during CO oxidation at low temperatures. Generally, nanomaterials with the high surface area are regarded as an ideal material for this application. The high surface area gives a greater tendency for active species to contact with reactants, and that gives an improved catalytic performance. There are various morphologies reported for CO oxidation performance. For example, nanotubes have inner and outer surfaces that supply active sites for the reactants, and that leads to better performance in

CO oxidation [15]. On the other hand, nano-sized particles also have a high surface area, but they show poor CO oxidation performance. Nanorods with low surface areas show better performance in CO oxidation compared to the nano-sized particles [16]. This different behavior of various morphologies is mainly because of the exposed planes. For instance, the nanoparticles dominantly have (111) exposed planes and nanorods have (100) and (110) planes on the edges. The (100) and (110) planes are regarded to be more active than (111) plane, so nanorods have better catalytic activity for CO oxidation compared to nano-sized particles.

Doping foreign elements into ceria lattice can significantly change the inherent chemical and physical properties of ceria. Sn-, Pr-, Y-, Zr-, and La-doped ceria were used for CO oxidation and the result was reported by Xiao et al. [17]. They synthesized a flower-like structure, and the catalytic activities for CO oxidation of all dopants were recorded as shown in Figure 2.

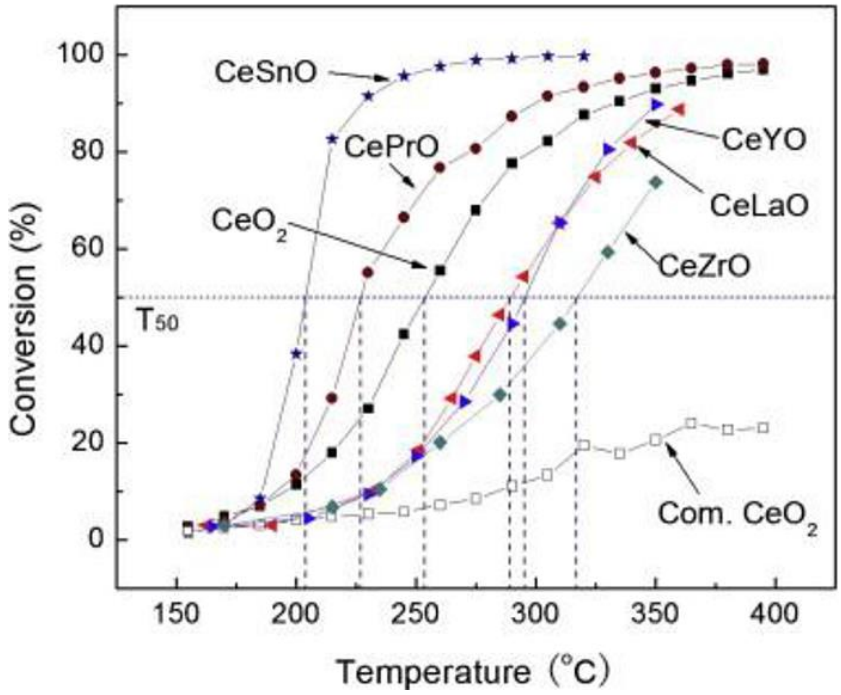

Figure 2. CO oxidation plots of ceria samples [17].

The figure 2 shows the doping of Sn and Pr improved the catalytic activities of the ceria nanoflower structure and the variable valence states of Pr and Sn is the main reason for that. The doping of La, Y, and Zr in ceria did not show better catalytic activities than pure ceria, and the stable valence states of dopants explain the trends. Also, doping cations with stable valence state partly suppress the redox reactions, and it eventually suppresses the oxygen storage capacity of the cations.

Electrospinning Technique

2. 2. 1 Electrospinning Process

Electrospinning technique employs electrostatic forces to synthesize fine fibers with a diameter ranging from nanometer to micrometer using polymer solutions. This technique gives fibers with a larger surface area than ones synthesized using conventional spinning processes. A DC (direct current) voltage of several tens of kV is required to provoke the electrospinning. Generally, electrospinning is conducted at room temperature and the general set up of electrospinning is given in Figure 3. Electrospinning set up consists of a spinneret, a high voltage power supply, and a collecting plate. An anode is connected to the spinneret and a cathode is connected to the collecting plate. So, when power is supplied to the system, the electric field is generated between the two electrodes. The electric field gives charge into a polymer solution, which is then accelerated towards a collecting plate of opposite polarity [8]. A precursor solution is synthesized by dissolving some polymers in some solvents before electrospinning. The polymer solution is then loaded into a syringe tube for electrospinning. This process should be conducted in chambers with a ventilation system since some polymers give off harmful smells [18]. In this process, a polymer solution held at the end of a syringe tip by its surface tension is subjected to

an electric field and an electric charge is generated on the solution surface. When the electric field is strong enough, the surface tension forces are overcome by the repulsive electrical forces. In the end, a charged jet stretching is discharged from the tip of the Taylor cone and unstable whipping of the jet stretching is generated in the space between the syringe tip and the collector plate which leaves polymer fibers on the plate with the evaporation of the solvent [19]. The Taylor cone is generated because of both coulombic and repulsive electrostatic forces alter the shape of the solution droplet into a cone-shaped meniscus, which is known as the Taylor cone. The jet is stable at the tip of the spinneret, but instability starts after that. Electrospinning is a simple process to produce fiber formation.

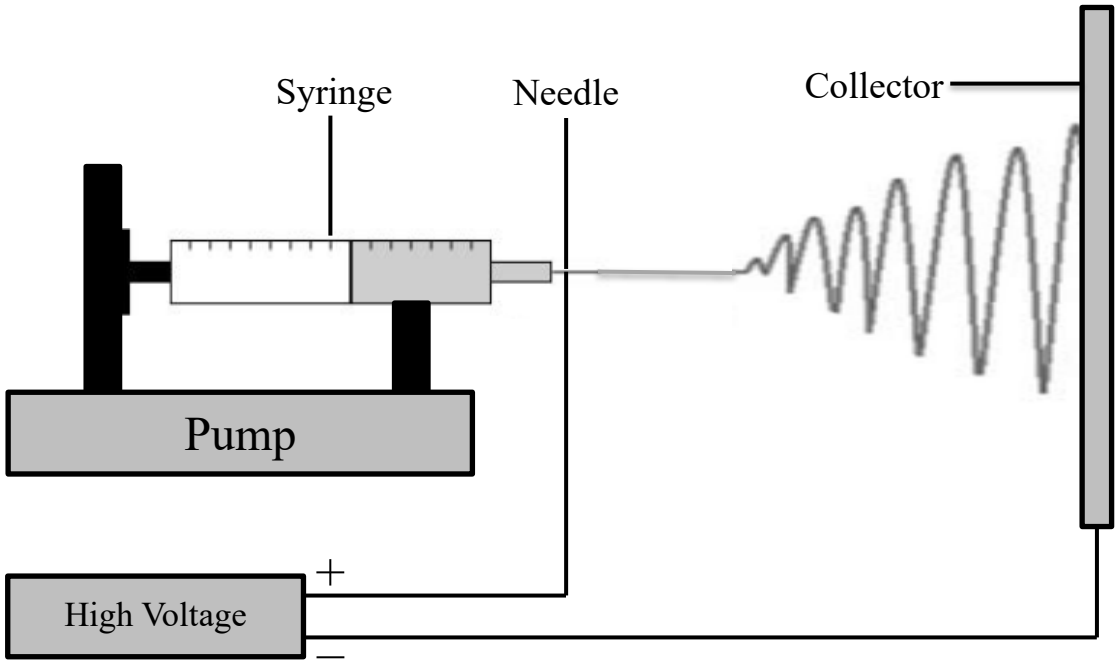

Figure 3. The schematic diagram of the electrospinning set up.

2. 2. 2 Taylor Cone

The creation of fibers by electrospinning is by stretching the continuously fed viscous solution jet with electrical shear stress. Stretching happens when the electrostatic coulombic forces caused by the gradient electric potential overcomes the cohesive intermolecular forces that keep the liquid droplet based on surface tension. Both coulombic and repulsive electrostatic forces deform the shape of the droplet into a conical shape, generally known as “Taylor cone” [20]. The electrified capillary jet is discharged from the Taylor cone and it develops into a straight segment. Then it breaks into a series of thinner streams developing under whipping instability. Each thinner jet goes through a continuous elongation process and bending instabilities as it travels to the collector. The thinning process is accompanied by the solvent evaporation and that allows thinner jets to solidify into nanofibers.

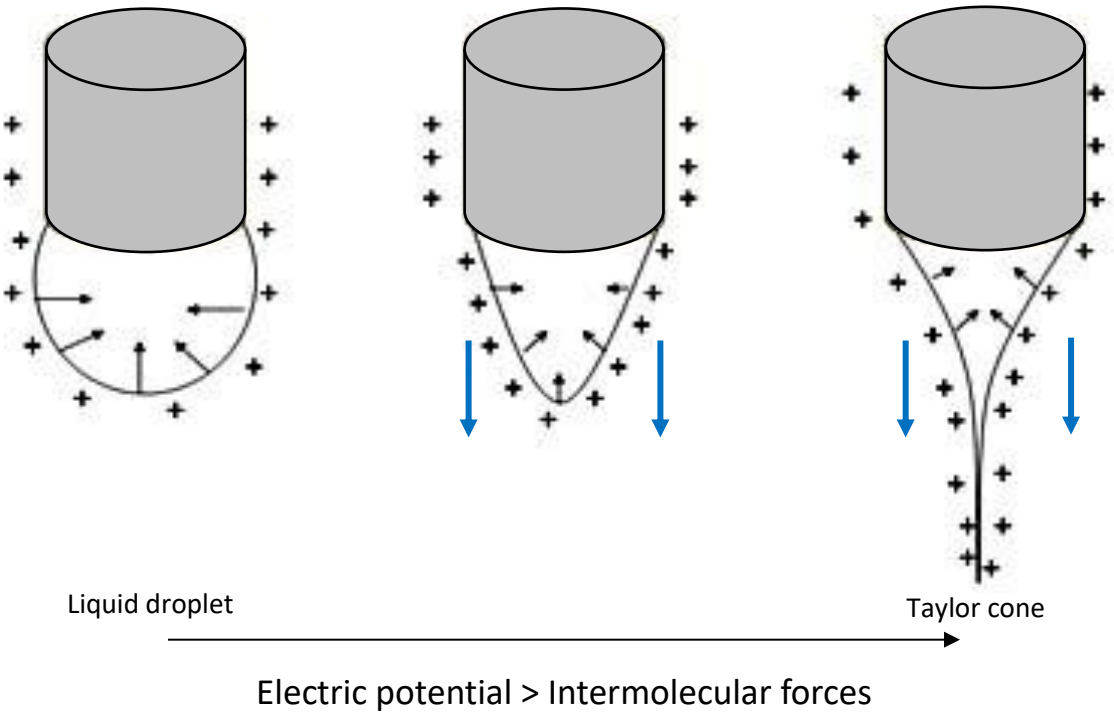

Figure 4. The development of Taylor cone [21].

2. 2. 3 Electrospinning-solution Properties

The main physical solution parameters that control the electrospinning process are the viscosity, electrical conductivity, and surface tension. Based on the range of polymer concentrations, solution viscosity is determined, and it enables the production of continuous and beaded-free fibers. Typically, solutions with low polymer concentrations (< 0.3 wt%) are dripped due to insufficient polymer chain entanglement. Increasing the polymer concentration yields fibers with greater diameters [22]. The polymer concentration is related to the viscosity, and both the polymer amount and molecular weight can be adjusted to attain an appropriate range of solution viscosities for electrospinning. In opposition to viscosity, the surface tension parameter is less sensitive to changes in the polymer concentrations but somewhat affected by its molecular polarity and the solvent phase composition [23]. In fact, the shear electrostatic repulsive forces must surmount the weak intermolecular forces that hold the solution droplet for electrospinning to have a continuous jet stretching. Therefore, a high surface tension suppresses the electrospinning process by damaging the jet stretching. However, adding some surfactant [24] and adjusting the solvent mixture composition [25] have been reported as adequate ways to produce uniform fibers by reducing the surface tension of the solution. Other than the viscosity and surface tension, the electrical conductivity also affects the uniformity and diameter of fibers for electrospinning. The electrical conductivity reflects the distribution of the charge density and the overall ionic strength of the solution when it is exposed to the electrical field. The electrical conductivity of the solution is largely dependent on the polymer type [26], the dielectric properties and solvent composition [27] and ionic surfactants [24]. Generally, enhancing the electrical conductivity of the polymer solution is reported beneficial for synthesizing ultrathin fibers (few tens of nanometers in diameters) and for suppressing beads [28].

2. 2. 4 Key Apparatus and Ambient Variables

Other than the physical properties of the polymer solution, adjusting the following key process variables is significant to control the morphology of the electrospun fibers.

1) Feed rate. The electrospinning process enables the production of nano-scaled fibers. The feed rate that the solution is coming out of the syringe is a significant factor since it determines the material transferred to the stretching region. Controlling the solution feed rate is important since it affects not only the fiber diameter but also the productivity of the electrospinning process. The rate is generally decided with a syringe pump, and an appropriate solution flow rate should be ensured to keep a stable Taylor cone at a given voltage. Usually increasing the flow rate leads to the production of larger fibers. It may eventually produce beads because of feed dynamics outrunning that governing the jet splitting and polymer solution polarization [27].

2) The electric field strength. The value of the critical voltage is based on the solution properties such as the solution viscosity and the polymer molecular weight. In addition, to avoid solution dripping or wagging, the value of the applied voltage and the distance between the syringe tip and the collector plate must be decided accordingly. The average electric field value to maintain a stable jet stretching is generally under 4kV/cm [29].

Xia et al. [30] studied the effect of different operating voltages. A more stable solution jet could be attained arranging from 8 kV to 25 kV and an optimum value was 17 kV. Beyond the voltage range, the jet uniformity was lost, and poor quality of fibers was attained.

3) Environmental parameters. Relative humidity, temperature, and air velocity during the electrospinning process are important parameters that impact both the morphology and the diameter. For example, when the working temperature gets higher, the fiber diameters get smaller since the higher temperature leads to faster solvent evaporation. However, the fast

solvent evaporation can cause clogging of the syringe tip, so processing parameters such as the polymer solution viscosity and working voltage should be balanced to avoid operational constraints. Relative humidity also affects fiber formation. When the relative humidity value is low, the solvent evaporates faster, resulting in the formation of fibers with smaller diameters. In addition, when the relative humidity value is high, the fibers with higher diameters are formed [31]. The electrospinning process cannot be performed when the relative humidity is beyond a threshold value because an arching and corona discharge may happen [32]. Based on the setups, exotic environment different environmental conditions can be introduced to control the fiber morphology. For example, introducing a heating element near the collecting plate to control the temperature can adjust the conditions for solvent evaporation, allowing the pore size distribution and porous structure of the fibers [33].

2. 2. 5 Effect of Calcination Temperature

Xia et al. [30] studied the effect of heat-treatment temperatures. Fibers with a diameter as thin as 50 nm were calcinated at 500, 800, 1000 and 1200 ºC and the one-dimensional structure were well-conserved up to 800 ºC. Nanofibers calcinated above 800 ºC lost its one-dimensional structure and became coarse because of uncontrolled and irregular growth of particles.

Electrospinning of Ceria Related Nanofibers

2. 3. 1 Pure Ceria Nanofibers

In 2005, Yang et al. [34] first introduced the synthesis of pure ceria nanofibers using electrospinning method. Cerium (III) nitrate hexahydrate as a precursor and 7wt% polyvinyl alcohol (PVA, MW 80,000) as a polymer. The electrospinning setup consisted of a plastic

capillary and a copper pin that was connected to a voltage source. A grounded rotating drum covered with aluminum foil was used as a counter electrode for fiber collection. The PVA and cerium nitrate composite solution was electrospun at 7kV, synthesizing a dense web of nanofibers. The X-ray diffraction (XRD) of the composite fibers had a broad diffraction peak at $2\theta=20°$ showing the (101) plane of semi-crystalline PVA. The composite fiber mats were dried for 8 hours at 90 ºC, then heated at 500 ºC for 6 hours by a rate of 4 ºC/min. In that way, highly crystalline pure ceria nanofibers with a diameter ranging from 50 to 100 nm were achieved for the first time.

Luepong et al [35]. studied the effect of i-propanol (IPA) and water as co-solvents on the morphology of electrospun fibers. In the study, the amount of IPA was changed from 0 to 50 wt% to control the viscosity and surface tension of the composite mixture. The composite fibers were synthesized by electrospinning technique at 15 kV and 7 cm of the needle tip to collector distance. The viscosity and solution surface tension were found to heavily change the quality of the fibers by affecting the forming of beads. When the IPA content was as high as 50 wt% in the solvent system, the surface tension was decreased leading to continuous and smoother fibers, while using only water as solvent yielded jammed fibers. Using co-solvent with IPA 50 wt%, continuous and smooth sub-micron scale ceria fibers with a diameter of 600 nm were obtained upon calcination. The XRD and EDS analysis confirmed the formation of the ceria phase with the fluorite cubic lattice.

Other electrospinnable polymers such as polyvinylpyrrolidone (PVP), polyvinyl butyral (PVB) [36, 37], have been studied to improve the quality of the synthesized electrospun mat and tailor the fiber structure. For instance, both porous and hollow structures could be achieved by Qizheng et al. [38] by using PVP/cerium nitrate composites. Usually, the water from the composite fibers

diffuses on the surface and evaporate during the post drying or heat treatment stage. The heat treatment leads to volatilization and combustion of the PVP and nitrate species and cerium ions are oxidized to ceria crystallites. These crystallites initially agglomerate to small nanoparticles, then grow by sintering and are ultimately combined to form hollow-centered and porous nanofibers.

2. 3. 2 Ceria Based Mixed Metal Oxide (MMO) Nanofibers

Crystalline ceria is known for its synergistic textural and structural promoter roles in MMO catalysts, leading to increased oxygen storage capacity, improved redox cyclability and enhanced thermomechanical stability. The textural promotion role can be related to the great mechanical and thermal resistance that can be attained when ceria is mixed with other metal oxides. Furthermore, the structural promotion role can be attributed to the evolution of crystalline oxides with several lattice defects leading to more active centers. Based on these features, the synthesis of ceria based MMO nanofibers using electrospinning has been extensively studied over the last few years. Transition metals, rare-earth metals or post-transition metals have been used for ceria based MMO. The production strategy of ceria based MMO nanofibers generally combines an electrospinning step with a post-sintering process. The electrospinning solution generally consists of metal salts and spinnable polymers, but some stabilizing additives like acids can be added. The metal salts are dissolved in a polymer mixture and make a homogeneous sol-gel. The solubility of transition metals in ceria lattice is well-known to improve its oxygen storage capacity, redox stability, and electrical conductivity. Sonsupap et al. [39] produced Fe-doped ceria nanofibers with exotic properties like room temperature ferromagnetism. In this work, the precursor solution was produced by mixing a certain amount of cerium nitrate hexahydrate, iron

nitrate nonahydrate, and PVP in DMF. The composite fibers were calcined for 3 hours in the air at 800 Celsius to synthesize 30-60 nm diameter nanostructures. The electrospun fibers showed a diamagnetic behavior and the magnetization increased along with the calcination temperature, reaching up to 0.0923 emu/g. The XPS analysis of the calcined structure showed the presence of mixed Fe^{3+}/Fe^{2+} species and Ce^{4+}/Ce^{3+} oxidation states on the surface. The ferromagnetism was correlated with the spin electrons of Fe^{3+} and Ce^{3+} species, and its origin was related to defects within the mixed metal oxide and presence of oxygen vacancies. Fe-doped ceria nanofibers can be used to advance magnetically recoverable catalysts.

Copper-doping is one of the most effective ways to improve its selectivity in CO oxidation because of the synergistic redox interactions between copper and cerium [40]. Xu et al. synthesized Cu-doped ceria nanofibers using cerium nitrate hexahydrate, copper acetate monohydrate, PVP and a hydro-alcoholic solvent system. The composite fibers were synthesized in a standard electrospinning setup and then calcined for 4 hours at 550 Celsius to make it pure mixed metal oxide nanofibers. The nanofibers had 6 times higher BET surface area compared to nanoparticles obtained by co-precipitation. Both XRD and HR-TEM studies on the nanofibers showed the existence of a Cu dispersed fluorite-type ceria structure. Luo et al. [41] compared the structure-to-performance of their Cu-doped ceria nanofibers and surfactant-templated catalysts. The electrospinning precursor solution consisted of cerium nitrate hexahydrate, copper nitrate trihydrate and PAN dissolved in DMF. The composite fibers were calcined for 4 hours at 500 Celsius in the air to yield pure mixed metal oxide nanofibers. The catalyst based on the surfactant-templated (ST) method using cetyltrimethylammonium bromide was used for a comparison purpose. The XRD analysis showed traces of the CuO phase from the ST-based material, while no bulk CuO peaks were identified from the electrospun nanofibers. This

comparison demonstrates the homogeneity level that can be attained in a multi-component solid solution using the electrospinning technique.

Noon et al. synthesized La-doped ceria nanofibers using electrospinning technique. The nanofibers have the potential to be used in advanced oxidative methane coupling. The electrospinning precursor solution consisted of cerium/lanthanum nitrate hexahydrate, PVP, water and ethanol. Then, composite fibers are produced using the electrospinning technique and calcined at 650 Celsius to make it mixed metal oxide fibers. The obtained La-doped ceria nanofibers have 50-75nm diameter with negligible internal porosity. The XRD analysis of the calcined nanofibers showed very broad and short peaks with no impressive crystalline pattern, confirming the formation of a solid solution.

Doped Ceria Nanofibers

2. 4. 1. Carbon Monoxide (CO) and Ceria Support

The continuous technological progress over the past century has contributed to a deterioration of natural resources, thereby numerous hazardous components have been widely given off into the environment. Among them, CO is a prominent one. CO is a poisonous, odorless, colorless gas, and exposure to CO can trigger symptoms including nausea, headaches, and even death. The emission of CO is mainly because of the incomplete combustion of the automobile engine during transportation. Aside from this, CO is also given off PEM fuel cells, indoor air cleaning, closed-cycle CO_2 lasers, mounting petrochemical industries, and iron smelting. [42, 43]. It is very important to get rid of CO in our environment, and researchers are working on the development of catalysts to effectively remove CO. To save energy of the process, identifying catalysts that can get rid of CO at low temperatures is important. Noble metals such as Pd, Pt, Rh are known

for the most effective oxidation catalysts to get rid of CO [44]. However, there are major problems for using these catalysts including scarcity, high cost, and having inferior thermal stability at high temperatures which inhibit their applications for CO oxidation [45]. However, there are common and low-cost metal oxide catalysts to be used alternatively. Transition-metal (TM) catalysts can be great alternatives for noble metals because of their abundance and low-cost and they show great catalytic activity based on the metal.

The use of support catalysts is important since it can increase the interactions and stability between the support and dopants. Ceria catalyst has been recognized as a great support for CO oxidation because it has a high density of oxygen vacancy defects and Ce^{4+}/Ce^{3+} redox system with high oxygen storage capacity [46]. However, pure ceria is insecure at high temperatures because the gradual agglomeration of its particles results in a decreased oxygen storage capacity and eventual deactivation [47]. As a solution, solid solutions were formed by doping other cations into ceria lattice and they showed excellent performance because of the newly generated mixed oxide phases or doping-generated structural defects [48]. For example, Transition metals can be used as dopants to increase the catalytic activity of ceria by replacing Ce ions in the ceria lattice. Zhou et al. studied the lattice substitution of ceria with Cu, Fe, Mn, Ni, and Co for catalytic activity, and the lattice substitution with Cu had the best catalytic activity [49]. It has been known that the introduction of dopant cations into ceria lattice could increase the mobility of oxygen ions through the lattice oxide and provide high oxygen ion conductivity for the material, therefore forming higher oxygen vacancies to enhance the redox properties of the material [50, 51]. Ceria is great support not only for CO oxidation but also for NO_x reduction and water-gas shift reactions, and it has been studied extensively to improve catalytic activity [52, 53].

2. 4. 2 Ceria-based Copper Oxide Catalysts

Copper oxide catalysts are used for a lot of applications such as soot oxidation [54], preferential CO oxidation (PROX) [55], low-temperature CO oxidation [56], and water-gas shift (WGS) reaction [57]. Among these, $CuO\text{-}CeO_2$ catalysts have been widely used for CO oxidation or PROX because of their big potential to be used in fuel cell applications. Recent studies have shown that $CuO\text{-}CeO_2$ catalysts could replace the noble metals for CO oxidation in the future because of their high activity and low-cost [58].

There have been a lot of studies on the application of $CuO\text{-}CeO_2$ catalysts for CO oxidation. Jung et al. synthesized $CuO\text{-}CeO_2$ catalysts using a coprecipitation method and the best catalytic activity was achieved when the catalyst was calcined at 700 °C. After the calcination, the most stable Cu-Ce-O solid solution was formed, on which CO could chemisorb the best [59]. Martinez-Arias et al. studied the catalytic activity of $CuO\text{-}CeO_2$ and $CuO\text{-}ZrCeO_4$ catalysts for CO oxidation and $CuO\text{-}CeO_2$ catalyst was more active. That was mainly because of the better reducibility of sites at the interface between the CuO and CeO_2 [60]. Luo et al. studied surfactant-templated $CuO\text{-}CeO_2$ catalysts for CO oxidation and they showed great catalytic activity. It was also concluded that the active sites for the reaction were the finely dispersed CuO species [56].

There seems to be an agreement in papers that both the CuO and CeO_2 play significant roles for CO oxidation and the reaction takes place at the active sites between CuO and CeO_2. Liu and Stephanopoulos suggested a CO oxidation reaction model, which CeO_2 offers the oxygen source through a swift redox cycle of Ce^{4+}/Ce^{3+} and Cu^{+} species provide active sites for CO chemisorption. The interaction between CuO and CeO_2 stabilizes the formation of Cu^{+} species [61]. Martinez-Arias et al. suggested that the extent of oxidation of copper, in which both

partially reduced, and fully oxidized states were greatly affected by the interaction with CeO_2 support. In addition, the redox properties and the partially reduced state of the copper oxide phase are two elements contributing to CO oxidation [60].

The catalytic activity increases as the Cu content increases, however, the excessive amount of Cu causes phase separation from the ceria lattice and eventually decrease the catalytic activity. Therefore, an optimal concentration of dopants should be used to achieve the best catalytic activity. Mai et al. reported that copper doped ceria has higher catalytic activity than copper oxide and pure ceria [62]. Therefore, in order to achieve the best catalytic activity, Cu-doped ceria must exist as a single phase, and copper oxide should not exist on the ceria surface as a secondary phase. These preceding studies have given us an extensive understanding of the nature of CuO-CeO_2 catalysts for CO oxidation.

2. 4. 3 Ceria-based Manganese Oxide Catalysts

Although the doped ceria systems have been widely studied, the doping with Mn into the ceria lattice is still to be studied. Mn is one of the most common transition metals and Mn^{3+} has ionic radii of 0.0645 nm, which is small compared to Ce^{4+} (0.097 nm). Manganese oxide catalysts are low-cost, durable and highly active for CO oxidation reactions, especially at low temperatures [63]. The Mn-based oxides were used widely for numerous catalytic reactions such as ammonia oxidation, decomposition of NO_x, and combustion of volatile organic compounds, and the greater performances were verified by the variable valences of Mn [64]. Because of the possibility of variable valences of Mn as well as the redox properties associated with Ce, the MnO_x-CeO_2 could be appealing materials for further investigation for both the spectral and structural understanding of the system [65]. For example, they can be utilized as heterogeneous

catalysts for the abasement of pollutants in the gas and liquid phases, such as oxidation of formaldehyde and acrylic acid and the catalytic reduction of NO [66], which show greater catalytic activity than those of pure CeO_2 and MnO_x. Recently, Delimaris and Ioannides found that toluene could be nearly oxidized at a temperature of 523K [67]. Xingyi et al. also found that chlorobenzene could be catalytically combusted using MnO_x-CeO_2 catalysts at temperatures of 527K [68]. Zhang et al. synthesized monodisperse Mn-doped ceria nanoparticles using a facile template-free solvothermal method and Mn-doped ceria had better catalytic activity than pure ceria towards CO oxidation [69]. Venkataswamy et al. synthesized Mn-doped ceria catalysts with high surface area using the co-precipitation method and $Ce_{1-x}Mn_xO_{2-\delta}$ (x=0.3) catalyst calcined at 773K had superior catalytic activity for low-temperature CO oxidation. It could be mainly ascribed to the reducibility, high surface area, high oxygen storage capacity and more surface oxygen defects [70]. Also, The observed uncommon catalytic performance of MnO_x-CeO_2 catalysts was attributed to the formation of massive amounts of oxygen species (O^{2-}, O_2^{2-}, O^-, etc.) on the Mn-doped ceria surface [71].

2. 4. 4 Ceria-based Iron Oxide Catalysts

Iron and cerium mixed oxides have attracted some attention since iron oxides and ceria are both has great importance in catalysis. Fe doped ceria systems present an impressive improvement of their catalytic activity for CO oxidation compared to the pure ceria due to the Fe-Ce synergy, which is ascribed to the combination of the redox behavior of iron (Fe^{3+}/Fe^{2+}) and cerium (Ce^{4+}/Ce^{3+}). Perez-Alonso et al. have studied the Fe-Ce interactions in several Fe-Ce mixed oxides synthesized with coprecipitation [72-74]. The catalytic performances were evaluated in the Fisher-Tropsch synthesis and N_2O decomposition, and from these studies, cubic ceria-like

and hematite-like solid solutions were formed in the Fe-Ce systems. These materials displayed better catalytic activity than the pure ceria and iron oxides. Bao et al. reported the synthesis of Fe_2O_3-CeO_2 catalysts with different iron concentrations using the coprecipitation method with urea as a precipitation agent [75]. They found that the composite material has a limit for the solid solution formation, and it was around 30 molar percentage of Fe. The 10mol% Fe-doped ceria composite exhibited the best catalytic activity for CO oxidation, which is ascribed to the highest amount of oxygen vacancies of the composite. Laguna et al. synthesized a series of Fe-doped ceria catalysts using the microemulsion method. 10 at% Fe-doped ceria has the greatest amount of oxygen vacancies, which comply with the best catalytic activity of CO oxidation for that concentration [76]. Wang et al. found that the oxygen storage capacity and rate of ceria is greatly improved by Fe-doping based on the TPR and XPS analysis, and that complies well with the fact that the textural and structural properties are greatly adjusted by Fe-doping [77]. Qiao et al. synthesized a series of $Fe_xCe_{1-x}O_2$ catalysts and found that $Fe_{0.1}Ce_{0.9}O_2$ catalyst had the greatest catalytic activity for CO and CH_4 oxidation [78]. Based on the previous findings, Liu et al. studied Fe-doped ceria with the purpose of a theoretical understanding of the interaction of the CO with the ceria (111) surface and how Fe-doping alters the catalytic activity [79]. They found that the formation energy of oxygen vacancy of the Fe-doped ceria (111) surface is decreased compared to the undoped system. Also, the Fe dopant causes large disruption on the electronic and geometric structure of $Ce_{0.92}Fe_{0.08}O_2$ (111) surface which promotes the CO oxidation reaction and formation of oxygen vacancies on the surface.

2. 4. 5 Ceria-based Cobalt Oxide Catalysts

Some metal oxides are known for their catalytic activity towards CO oxidation and Co_3O_4 is active for CO oxidation in the absence of moisture [80]. Co_3O_4 is appealing as an oxidation catalyst due to the existence of mobile oxygen in it [81, 82]. The great catalytic activity of Co_3O_4 on oxidation reactions could be because of the relatively low enthalpy of vaporization of O_2 [83]. That means that the reactive oxygen can be easily formed from the lattice oxygen since the Co-O bond strength is relatively weak. For this reason, many researchers have studied the catalytic activity of Co_3O_4 for CO oxidation. Co_3O_4 was reported to exhibit morphology-dependent catalytic activity [84]. Co_3O_4 nanostructures with various shapes such as nanorods, nanocubes, nanobelts, and others have synthesized to reveal crystal planes with various compositions [85]. The (011) planes have the superior activity for CO oxidation compared to (001) and (111) planes, and it turned out that the (011) planes mainly comprise Co^{3+} cations and (001) and (011) planes contain only Co^{2+} cations. The great amount of Co^{3+} cations was relevant to the superior catalytic activity, and Co^{3+} cations were also claimed to be the active sites for methane oxidation [83, 84]. Iablokov et al. synthesized Co_3O_4 nanoparticles with a size in the range of 3.5 and 12.2 nm to study the particle size effect of Co_3O_4 nanoparticles for CO oxidation [86]. They found that the reaction is structure-sensitive, and the maximum reaction rate was achieved by the sample with particle sizes between 5 and 8 nm.

For Co-doped ceria catalysts, Kang et al. synthesized a series of metal-doped ceria composite using the co-precipitation method to study the catalytic activity of CO oxidation [87]. Among them, CoO_x/CeO_2 exhibited the best catalytic activity compared to other catalyst systems. Also, Jampaiah et al. synthesized Mn, Co, and Ni-doped ceria nanorods catalysts and Co-doped ceria

had the best catalytic activity towards CO oxidation [88]. They found that doping with cobalt increased the formation of surface oxygen vacancies using Raman spectroscopy.

2. 4. 6 Ceria-based Nickel Oxide Catalysts

With rich reserves and great redox property, nickel oxide has been widely studied for catalysts. It has been known that the addition of nickel into ceria lattice could improve the oxygen diffusion of ceria by increasing the oxygen vacancies, therefore contributes to favorable performances of oxidation reactions. Qiao et al. synthesized MO_x-CeO_2 (M = Cu, Fe, Co, Mn, and Ni) catalysts for CH_4 wet combustion, and they found that the NiO-CeO_2 catalyst had the best durability [89]. Tang et al. studied the details of the chemical compositions and textural properties of the mesoporous NiO-CeO_2 catalysts and correlated them with the catalytic activity for CO oxidation [90]. They synthesized a series of nickel-cerium mixed oxides using KIT-6 as a template and they found that the size and distribution of mesopores were rarely affected by the amount of nickel introduced. The catalytic activity for CO oxidation was decreased with the increasing nickel content in the samples, and this could be ascribed to the interaction between nickel and ceria.

Papaioannou et al. synthesized exsolved Fe-Ni bimetallic alloy nanoparticles and used them to study the catalytic activity of CO oxidation [91]. They found that the exsolved Ni nanoparticles can greatly increase the catalytic activity and long-term stability.

Li et al. synthesized Ni-Ce(La)O_x and Cu-Ce(La)O_x catalysts using the urea co-precipitation-gelation method and they were examined as water-gas shift catalysts [92]. They found that both catalysts have great catalytic activity and the Cu-Ce(La)O_x catalyst had better activity. Also, they

found that high metal content leads to the bulk particle formation and it rarely contributed to the catalytic activity.

2. 4. 7 Ceria-based Lanthanum Oxide Catalysts

When ceria is doped with lanthanide cations such as Gd^{3+}, La^{3+}, and Y^{3+}, an enhancement of the concentration of oxygen vacancies in the ceria lattice is expected. This feature improves the migration of oxygen ions through the ceria lattice, thereby the high oxygen ion conductivity [93]. Also, it was reported that the existence of oxygen vacancies is correlated to the increase of the catalytic performances of the materials, ascribed to the interaction of the reactive gas with surface defects [94, 95]. Hernandez et al. mixed ceria with La, Eu and Gd using coprecipitation and measured catalytic activities toward CO oxidation [96]. All the materials showed better catalytic activity for the CO oxidation compared to the undoped ceria. Also, Signhania synthesized La, Pr, Nd and Pm-doped ceria nanoparticles using the citric acid-aided sol-gel method and used them to measure the catalytic activities of CO oxidation [119]. Nanoparticle materials with high surface area (190 – 198 m^2/g) were successfully synthesized and La-doped ceria showed the best catalytic activity compared to the other doped materials. However, it has also been reported that La doping was not increasing the catalytic activity of ceria. Zhou et al. synthesized La and Cu-doped ceria nanosheets using a facile and one-step complexing coprecipitation (CC) method and used them to measure catalytic activity towards CO oxidation [97]. The Cu-doped ceria showed high catalytic activity (T_{50} = 83 ºC), but La-doped ceria showed even lower catalytic activity compared to the undoped nanosheet material. In this thesis, I used La as a dopant for ceria and measured the catalytic activity towards CO oxidation to study the effects of dopant La for CO oxidation reaction.

2. 4. 8 Metal-doped Ceria for CO Oxidation

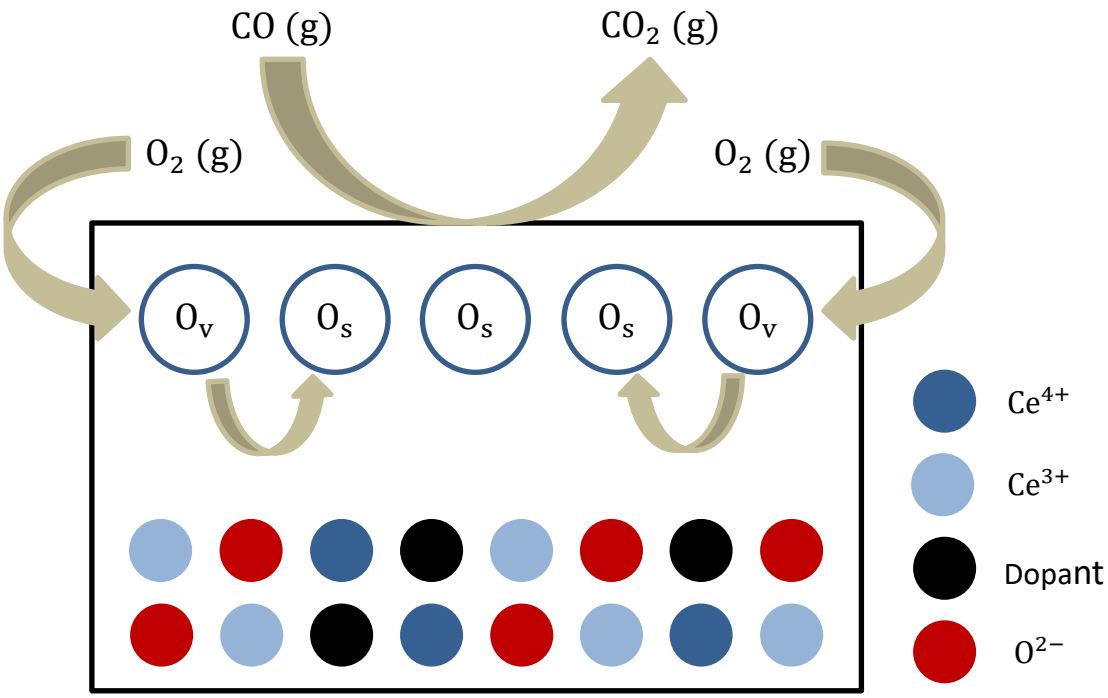

Figure 5. Proposed CO oxidation mechanism over metal-doped ceria catalysts [98].

Oxygen storage capacities (OSC) are an important factor to decide if a catalyst has good catalytic activities [98]. It gives information about the most available and active oxygen atoms in the catalyst. The incorporation of dopant ions will produce the formation of extrinsic oxygen vacancies within the ceria lattice in order to preserve the charge neutrality. Therefore, the defects created by the incorporation of dopant ions produce labile oxygen vacancies, leading to the high mobility of bulk oxygen species in the ceria lattice. That means the enhancement of the OSC and the catalytic activity of the metal-doped catalyst increases as the amounts of OSC increase.

CO Oxidation

2. 5. 1 Ceria Nanospheres and CO Oxidation

Ceria nanomaterials with various morphologies such as nanoparticles [99], nanorods [100], nanotubes [101] and mesoporous spheres [102] have been successfully synthesized through different methods. The synthesis of porous ceria hollow nanospheres has widely studied due to the advantages as catalytic materials for their superior structural properties, which is the hollow interior space enhances the spatial dispersion, and the pores effectively enhance the direct contact between catalysts and reactants. Wang et al. successfully synthesized ceria hollow nanospheres by using the carbon sphere and silica as hard templates [103]. However, this method requires a need to get rid of the templates, and in many cases, the template materials cannot endure under reaction conditions. Therefore, it is desirable to develop a facile, low-cost and template-free synthesis of porous ceria hollow nanospheres. Cai et al. successfully synthesized a template-free ceria hollow nanospheres, but the method requires two steps and calcination of ceria precursors at 500 °C [104]. Jiao et al. reported a one-step, template-free and low-cost synthesis of porous ceria hollow nanospheres. The synthesized ceria hollow nanospheres have a size of 135 nm and are consisted of ceria nanoparticles of about 3 nm. Their porous ceria hollow nanospheres have great potential as catalysts due to their unique porosity structures and high surface area. Additionally, Au was deposited to the ceria nanospheres and it showed great catalytic activity for CO oxidation [105].

2. 5. 2 CO Oxidation Reaction Mechanisms

A Langmuir-Hinshelwood (L-H) mechanism was used to define the CO oxidation reaction over CuO/CeO_2 catalyst by Liu and Stephanopoulos [61]. The characteristic trait of the mechanism is

that CO and O_2 are chemisorbed on the ceria surface before the reaction takes place [106]. It was considered that CO or O_2 adsorbs on reactive sites of catalysts prior to the CO oxidation reaction and Cu^+ ions serve as adsorptive sites for CO. However, kinetic studies of CO oxidation over CuO/CeO_2 demonstrate that the reaction rate is linearly related to CO partial pressure, but it is not related to O_2 partial pressure [61]. Therefore, that can be a proof for the oxygen gas is not directly involved in the reaction. Moreover, Sedmak et al. reported that CO can be oxidized even without O_2 gas in the gas phase using $Cu_{0.1}Ce_{0.9}O_{2-\delta}$ [107, 108].

From these findings, the Mars-van Krevelen mechanism is proposed and it is shown in figure 5. The characteristic trait of the mechanism is that products of reactions leave the solid catalysts' surface with one or more components of the catalysts' lattice [109]. The reaction involves (1) chemisorption of CO on dopant ions, (2) movement of the chemisorbed CO to the interface of dopant and ceria, (3) activation of O_2 on the oxygen vacancies in ceria and formation of lattice oxygen O^{2-} or active oxygen O_2^-, (4) reaction of chemisorbed CO and active oxygen and (5) refill of oxygen vacancies by oxygen gas [110].

2. 6 References

[1] Trovarelli, P. Fornasiero, "Catalysis by ceria and related materials Catalytic Science Series," *Imperial College Press* 12 (2013).

[2] N.V. Skorodumova, S.I. Simak, B.I. Lundqvist, I.A. Abrikosov, B. Johansson, "Quantum Origin of the Oxygen Storage Capability of Ceria," *Phys Rev Lett* 89 (2002) 166601.

[3] I.I. Soykal, H. Sohn, U.S. Ozkan, "Effect of Support Particle Size in Steam Reforming of Ethanol over Co/CeO_2 Catalysts," *ACS Catal* 2 (2012) 2335-2348.

[4] P.W. Dunne, A.M. Carnerup, A. Wegrzyn, S. Witkowski, R.I. Walton, "Hierarchically Structured Ceria-Silica: Synthesis and Thermal Properties," *J Phys Chem C* 116 (2012) 13435-13445.

[5] X.Tang, Y. Li, X. Huang, Y. Xu, H. Zhu, J. Wang, W. Shen, "MnOx–CeO2mixed poly oxidation of formaldehyde: Effect of preparation method and calcination temperature," *Appl Catal B* 62 (2006) 265-273.

[6] Z. Sun, E. Zussman, A. L. Yarin, J. H. Wendorff, A. Greiner, "Compound core-shell polymer nanofibers by co-electrospinning," *Adv Mater* 15 (2003) 1929–1933.

[7] D. H. Reneker, A. L. Yarin, H. Fong, S. Koombhongse, "Bending instability of electrically charged liquid jets of polymer solutions in electrospinning," *J Appl Phys* 87 (2000) 4531-47.

[8] D. Liang, B. S. Hsiao, B. Chu, "Functional electrospun nanofibrous scaffolds for biomedical applications," *Adv Drug Deliv Rev* 59 (2007) 1392–412.

[9] D. R. Schryer, B. T. Upchurch, B. D. Sidney, K. G. Brown, G. B. Hoflund, R. K. Herz, "A proposed mechanism for Pt/SnO sub x-catalyzed CO oxidation," *J Catal* 130 (1991) 314.

[10] L. Malavasi, C. A. J. Fisher, M. S. Islam, "Oxide-ion and proton conducting electrolyte materials for clean energy applications: structural and mechanistic features," *Chem Soc Rev* 39 (2010) 4370-4387.

[11] Z. L. Wang, X. D. Feng, "Polyhedral shapes of CeO_2 nanoparticles," *J Phys Chem B* 107 (2003) 13563-13566.

[12] J. A. Kilner, "Defects and conductivity in ceria-based oxides," *Chem Lett* 37 (2008) 1012-1015.

[13] C. T. Campbell, C. H. F. Peden, "Oxygen vacancies and catalysis on ceria surfaces," *Sci* 309 (2005) 713-714.

[14] S. Park, J. M. Vohs, R. J. Gorte, "Direct oxidation of hydrocarbons in a solid-oxide fuel cell," *Nature* 404 (2000) 265-267.

[15] C. Pan, D. Zhang, L. Shi, "CTAB assisted hydrothermal synthesis, controlled conversion and CO oxidation properties of CeO_2 nanoplates, nanotubes, and nanorods," *J Solid State Chem* 181 (2008) 1298-1306.

[16] Tana, M. Zhang, J. Li, H. Li, Y. Li, W. Shen, "Morphology-dependent redox and catalytic properties of CeO_2 nanostructures: nanowires, nanorods and nanoparticles," *Catal Today* 148 (2009) 179-183.

[17] G. Xiao, S. Li, H. Li, L. Chen, "Synthesis of doped ceria with mesoporous flower-like morphology and its catalytic performance for CO oxidation," *Microporous Mesoporous Mater* 120 (2009) 426-431.

[18] Z. M. Huang, Y. Z. Zhang, M. Kotaki, S. Ramakrishna, "A review on polymer nanofibers by electrospinning and their applications in nanocomposites," *Compos Sci Technol* 63 (2003) 2223–53.

[19] E. Adomaviciute, R. Milasius, "The influence of applied voltage on poly (vinyl alcohol) (PVA) nanofibre diameter," *Fibers Text East Eur* 15 (2007) 64–5.

[20] D.H. Reneker, A.L. Yarin, "Electrospinning jets and polymer nanofibers," *Polymer* 49 (2008) 2387–2425.

[21] K. Polychronopoulou, M. A. Jaoude, "Nano-architectural advancement of CeO2-driven catalysis via Electrospinning," *Surface Coatings Technol* 350 (2018) 245-280.

[22] J. Lin, B. Ding, J. Yu, "Direct fabrication of highly nanoporous polystyrene fibers via electrospinning," *ACS Appl Mater Interfaces* 2 (2010) 521–528.

[23] K. H. Lee, H. Y. Kim, M. S. Khil, Y. M. Ra, D. R. Lee, "Characterization of nano-structured poly (ε caprolactone) nonwoven mats via electrospinning," *Polymer* 44 (2003) 1287–1294.

[24] J. Zeng, X. Xu, X. Chen, Q. Liang, X. Bian, L. Yang, X. Jing, "Biodegradable electrospun fibers for drug delivery," *J Control Release* 92 (2003) 227–231.

[25] S. Theron, E. Zussman, A. Yarin, "Experimental investigation of the governing parameters in the electrospinning of polymer solutions," *Polymer* 45 (2004) 2017–2030.

[26] A. Greiner, J.H. Wendorff, "Electrospinning: a fascinating method for the preparation of ultrathin fibers," *Angew Chem Int Ed* 46 (2007) 5670–5703.

[27] L. Wannatong, A. Sirivat, P. Supaphol, "Effects of solvents on electrospun polymeric fibers: preliminary study on polystyrene," *Polym Int* 53 (2004) 1851–1859.

[28] X. Wang, B. Ding, J. Yu, J. Yang, "Large-scale fabrication of two-dimensional spider-web-like gelatin nano-nets via electro-netting," *Colloids Surf B* 86 (2011) 345–352.

[29] M.K. Leach, Z.-Q. Feng, S.J. Tuck, J.M. Corey, "Electrospinning fundamentals: optimizing solution and apparatus parameters," *J Vis Exp* (2011) e2494.

[30] Y. J. Xia, J. L. Song, D. N. Yuan, X. N. Guo, X. Guo, "Synthesis and characterization of one-dimensional metal oxides: TiO2, CeO2, Y2O3-stabilized ZrO2 and SrTiO3," *Ceram Int* 41 (2015) 533–545.

[31] J. Pelipenko, J. Kristl, B. Jankovic, S. Baumgartner, P. Kocbek, "The impact of relative humidity during electrospinning on the morphology and mechanical properties of nanofibers," *Inter J Pharmaceutics* 456 (2013) 125-134.

[32] G. Collins, J. Federici, Y. Imura, L.H. Catalani, "Charge generation, charge transport, and residual charge in the electrospinning of polymers: a review of issues and complications," *J Appl Phys* 111 (2012) 044701.

[33] C.H. Kim, Y.H. Jung, H.Y. Kim, D.R. Lee, N. Dharmaraj, K.E. Choi, "Effect of collector temperature on the porous structure of electrospun fibers," *Macromol Res* 14 (2006) 59–65.

[34] X. Yang, C. Shao, Y. Liu, R. Mu, H. Guan, "Nanofibers of CeO2 via an electrospinning technique," *Thin Solid Films* 478 (2005) 228–231.

[35] K. Luepong, P. Koombhongse, P. Kongkachuichay, "Ceria fibers via electrospinning process: the effect of co-solvent," *Chiang Mai J Sci* 37 (2010) 85–91.

[36] F. Berutti, A. Alves, C. Bergmann, F. Clemens, T. Graule, "Synthesis of CeO2 and Y2O3-doped CeO2 composite fibers by electrospinning," *Part Sci Technol* 27 (2009) 203–209.

[37] G.C. Pontelli, R.P. Reolon, A.K. Alves, F.A. Berutti, C.P. Bergmann, "Application of cerium oxide electrospun fibers in the catalytic combustion of methane," *Appl Catal A Gen* 405 (2011) 79–83.

[38] C. Qizheng, D. Xiangting, W. Jinxian, L. Mei, "Direct fabrication of cerium oxide hollow nanofibers by electrospinning," *J Rare Earths* 26 (2008) 664–669.

[39] S. Sonsupap, P. Kidkhunthod, N. Chanlek, S. Pinitsoontorn, S. Maensiri, "Fabrication, structure, and magnetic properties of electrospun Ce0.96Fe0.04O2 nanofibers," *Appl Surf Sci* 380 (2016) 16–22.

[40] M. Jobbágy, F. Marino, B. Schönbrod, G. Baronetti, M. Laborde, "Synthesis of copper-promoted CeO2 catalysts," *Chem Mater* 18 (2006) 1945–1950.

[41] Y. Luo, K. Wang, Y. Xu, X. Wang, Q. Qian, Q. Chen, "The role of Cu species in electrospun CuO–CeO2 nanofibers for total benzene oxidation," *New J Chem* 39 (2015) 1001–1005.

[42] H. Zhu, Z. Qin, W. Shan, W. Shen, J. Wang, "Low-temperature oxidation of CO over Pd/CeO2–TiO2 catalysts with different pretreatments," *J Catal* 233 (2005) 41–50.

[43] N. Imanaka, T. Masui, H. Imadzu, K. Yasuda, "Carbon monoxide oxidation at room temperature on Pt/CeO2–ZrO2–Bi2O3 catalysts," *Chem Commun* 47 (2011) 11032–11034.

[44] M.S. Chen, Y. Cai, Z. Yan, K. K. Gath, S. Axnanda, D. W. Goodman, "Highly active surfaces for CO oxidation on Rh, Pd, and Pt," Surf Sci 601 (2007) 5326-5331

[45] H.J. Freund, G. Meijer, M. Scheffler, R. Schlögl, M. Wolf, "CO Oxidation as a Prototypical Reaction for Heterogeneous Processes," *Angew Chem Int Ed* 50 (2011) 10064–10094.

[46] T. Montini, M. Melchionna, M. Monai, P. Fornasiero, "Fundamentals and Catalytic Applications of CeO2-Based Materials," *Chem Rev* 116 (2016) 5987–6041.

[47] B. M. Reddy, G. Thrimurthulu, L.Katta, "Structural Characteristics and Catalytic Activity of Nanocrystalline Ceria-Praseodymia Solid Solutions," *J Phys Chem C* 113 (2009) 15882–15890.

[48] S. Collins, G. Finos, R. Alcántara, E. del Rio, S. Bernal, A. Bonivardi, "Effect of gallia doping on the acid–base and redox properties of ceria," *Appl Catal A* 388 (2010) 202–210.

[49] L. Zhou, X. Li, Z. Yao, Z. Chen, M. Hong, R. Zhu, Y. Liang, J. Zhao, "Transition-Metal Doped Ceria Microspheres with Nanoporous Structures for CO Oxidation," *Sci Rep* 6 (2016) 23900.

[50] T. Li, G. Xiang, J. Zhuang, X. Wang, "Enhanced catalytic performance of assembled ceria necklace nanowires by Ni doping," *Chem Commun* 47 (2011) 6060–6062.

[51] X. Yao, C. Tang, Z. Ji, Y. Dai, Y. Cao, F. Gao, L. Dong, Y. Chen, "Investigation of the physicochemical properties and catalytic activities of Ce0.67M0.33O2 (M = Zr4+, Ti4+, Sn4+) solid solutions for NO removal by CO," *Catal Sci Technol* 3 (2013) 688–698.

[52] B. Liang, H. Duan, X. Su, X. Chen, Y. Huang, X. Chen, J. J. Delgado, T. Zhang, "Promoting role of potassium in the reverse water gas shift reaction on Pt/mullite catalyst," *Catal Today* 281 (2017) 319–326.

[53] C. Deng, Q. Huang, X. Zhu, Q. Hu, W. Su, J. Qian, L. Dong, B. Li, M. Fan, C. Liang, "The influence of Mn-doped CeO2 on the activity of CuO/CeO2 in CO oxidation and NO + CO model reaction," *Appl Surf Sci* 389 (2016) 1033–1049.

[54] B. M. Reddy, K. N. Rao, "Copper promoted ceria–zirconia based bimetallic catalysts for low temperature soot oxidation" *Catal Commun* 10 (2009) 1350-1353

[55] A. Horne, A. B. Hungria, P. Bera, A. L. Camara, M. FernandezGarcia, A. Martinez-Arias, L. Barrio, M. Estrella, G. Zhou, J. J. Fonseca, J. C. Hanson, J. A. Rodriguez, "Inverse CeO2/CuO Catalyst As an Alternative to Classical Direct Configurations for Preferential Oxidation of CO in Hydrogen-Rich Stream," *J Am Chem Soc* 132 (2010) 34-35

[56] M. F. Luo, J. M. Ma, J. Q. Lu, Y. P. Song, Y. J. Wang, "High-surface area CuO–CeO2 catalysts prepared by a surfactant-templated method for low-temperature CO oxidation," *J Catal* 246 (2007) 52–59.

[57] E. B. Fox, S. Velua, M. H. Engelhard, Y. H. Chin, J. T. Miller, J. Kropf, C. Song, "Characterization of CeO2-supported Cu–Pd bimetallic catalyst for the oxygen-assisted water–gas shift reaction," *J Catal* 260 (2008) 358-370.

[58] G. Avgouropoulos, T. Ioannides, "Selective CO oxidation over CuO-CeO2 catalysts prepared via the urea–nitrate combustion method," *Appl Catal A* 244 (2003) 155-167.

[59] C. R. Jung, J. Han, S. W. Nam, T. H. Lim, S. A. Hong, H. I. Lee, "Selective oxidation of CO over CuO-CeO2 catalyst: effect of calcination temperature," *Catal Today* 93-95 (2004) 183-190

[60] A. Martinez-Arias, M. Fernandez-Garcia, O. Galvez, J. M. Coronado, J. A. Anderson, J. C. Conesa, J. Soria, G. Munuera, "Comparative Study on Redox Properties and Catalytic Behavior for CO Oxidation of CuO/CeO2 and CuO/ZrCeO4 Catalysts," *J Catal* 195 (2000) 207-216.

[61] W. Liu, M. Flytzani-stephanopoulos, "Total oxidation of carbon monoxide and methane over transition metal-fluorite oxide composite catalysts: 2. Catalyst characterization and reaction-kinetics," *J Catal* 153 (1995) 317-332.

[62] H. Mai, D. Zhang, L. Shi, T. Yan, H. Li, "Highly active Ce1−xCuxO2 nanocomposite catalysts for the low temperature oxidation of CO," *Appl Surf Sci* 257 (2011) 7551– 7559.

[63] Y. Luo, Y. Q. Deng, W. Mao, X. J. Yang, K. Zhu, J. Xu, Y. F. Han, "Probing the Surface Structure of α-Mn2O3 Nanocrystals during CO Oxidation by Operando Raman Spectroscopy," *J Phys Chem C* 116 (2012) 20975-20981.

[64] Z. Chen, Z. Jiao, D. Pan, Z. Li, M. Wu, C. H. Shek, C. M. L. Wu, J. K. L. Lai, "Recent Advances in Manganese Oxide Nanocrystals: Fabrication, Characterization, and Microstructure," *Chem Rev* 112 (2012) 3833–3855.

[65] B. Murugan, A. V. Ramaswamy, "Nature of Manganese Species in Ce1-xMnxO2-δ Solid Solutions Synthesized by the Solution Combustion Route," *Chem Mater* 17 (2005) 3983-3993.

[66] Z. Wang, G. Shen, J. Li, H. Liu, Q. Wang, Y. Chen, "Catalytic removal of benzene over CeO2–MnOx composite oxides prepared by hydrothermal method," *Appl Catal B* 138–139 (2013) 253–259.

[67] D. Delimaris, T. Ioannides, "VOC oxidation over MnOx–CeO2 catalysts prepared by a combstion method," *Appl Catal B* 84 (2008) 303–312.

[68] W. Xingyi, K. Qian, L. Dao, "Catalytic combustion of chlorobenzene over MnOx–CeO2 mixed oxide catalysts," *Appl Catal B* 86 (2009) 166–175.

[69] X. Zhang, J. Wei, H. Yang, X. Liu, W. Liu, C. Zhang, Y. Yang, "One-Pot Synthesis of Mn-Doped CeO2 Nanospheres for CO Oxidation," *Euro J Inorg Chem* 2013 (2013) 4443-4449.

[70] P. Venkataswamy, K. N. Rao, D. Jampaiah, B. M. Reddy, "Nanostructured manganese doped ceria solid solutions for CO oxidation at lower temperatures," *Appl Catal B* 162 (2015) 122-132.

[71] W. Cen, Y. Liu, Z. Wu, H. Wang, X. Weng, "A theoretic insight into the catalytic activity promotion of CeO2 surfaces by Mn doping," Phys Chem Chem Phys 14 (2012) 5769–5777.

[72] F.J. Perez-Alonso, I. Melián-Cabrera, M. López Granados, F. Kapteijn, J. L. G. Fierro, "Synergy of FexCe1−xO2 mixed oxides for N2O decomposition," *J Catal* 239 (2006) 340–346.

[73] F. J. Pérez-Alonso, T. Herranz, S. Rojas, M. Ojeda, M. López Granados, P. Terreros, J. L. G. Fierro, M. Gracia, J. R. Gancedo, "Evolution of the bulk structure and surface species on Fe–Ce catalysts during the Fischer–Tropsch synthesis," *Green Chem* 9 (2007) 663–670.

[74] F. J. Pérez-Alonso, M. L. Granados, M. Ojeda, T. Herranz, S. Rojas, P. Terreros, J. L. G. Fierro, M. Gracia, J. R. Gancedo, "Relevance in the Fischer-Tropsch Synthesis of the Formation of Fe-O-Ce Interactions on Iron-Cerium Mixed Oxide Systems," *J Phys Chem B* 110 (2006) 23870–23880.

[75] H. Bao, X. Chen, J. Fang, Z. Jiang, W. Huang, "Structure-activity Relation of Fe2O3–CeO2 Composite Catalysts in CO Oxidation," *Catal Lett* 125 (2008) 160–167.

[76] O. H. Laguna, M. A. Centeno, M. Boutonnet, J. A. Odriozola, "Fe-doped ceria solids synthesized by the microemulsion method for CO oxidation reactions," *Appl Catal B* 106 (2011) 621-629.

[77] J. Wang, B. Zhang, M. Shen, "Effects of Fe-doping of ceria-based materials on their microstructural and dynamic oxygen storage and release properties," *J Sol-Gel Sci Technol* 58 (2011) 259–268.

[78] D. S. Qiao, G. Z. Lu, X. H. Liu, Y. Guo, Y. Q. Wang, Y. L. Guo, "Preparation of Ce1-xFexO2 solid solution and its catalytic performance for oxidation of CH4 and CO," *J Mater Sci* 46 (2011) 3500–3506.

[79] X. S. Liu, X. D. Wang, M. Yao, W. Cui, H. Yan, "Effects of Fe doping on oxygen vacancy formation and CO adsorption and oxidation at the ceria (111) surface," *Catal Commun* 63 (2015) 35-40.

[80] D. A. H. Cunningham, T. Kobayashi, N. Kamijo, M. Haruta, "Influence of dry operating conditions: observation of oscillations and low temperature CO oxidation over Co3O4 and Au/Co304 catalysts," *Catal Lett* 25 (1994) 257–264.

[81] J. Jansson, "Low-Temperature CO Oxidation over Co3O4/Al2O3," *J Catal* 194 (2000) 55-60.

[82] H. K. Lin, C. B. Wang, H. C. Chiu, S. H. Chien, "In situ FTIR study of cobalt oxides for the oxidation of carbon monoxide," *Catal Lett* 86 (2003) 63-68.

[83] M. Haneda, Y. Kintaichi, N. Bion, H. Hamada, "Alkali metal-doped cobalt oxide catalysts for NO decomposition," *Appl Catal B* 46 (2003) 473-482.

[84] X. Xie, Y. Li, Z. Q. Liu, M. Haruta, W. Shen, "Low-temperature oxidation of CO catalysed by Co3O4 nanorods," *Nature* 458 (2009) 746−749.

[85] L. Hu, K. Sun, Q. Peng, B. Xu, Y. Li, "Surface Active Sites on Co3O4 Nanobelt and Nanocube Model Catalysts for CO Oxidation," *Nano Res* 3 (2010) 363−368.

[86] V. Iablokov, R. Barbosa, G. Pollefeyt, I. V. Diessche, S. Chenakin, N. Kruse, "Catalytic CO Oxidation over Well-Defined Cobalt Oxide Nanoparticles: Size-Reactivity Correlation," *ACS Catal* 5 (2015) 5714-5718.

[87] M. Kang, M. W. Song, C. H. Lee, "Catalytic carbon monoxide oxidation over CoOx/CeO2 composite catalysts," *Appl Catal A* 251 (2003) 143-156.

[88] D. Jampaiah, P. Venkataswamy, V. E. Coyle, B. M. Reddy, S. K. Bhargava, "Low-temperature CO oxidation over manganese, cobalt, and nickel doped CeO2 nanorods," *RSC Adv* 6 (2016) 80541.

[89] D. Qiao, G. Lu, Y. Guo, Y. Wang, Y. Guo, "Effect of water vapor on the CO and CH4 catalytic oxidation over CeO2-MOx(M=Cu, Mn, Fe, Co, and Ni) mixed oxide," *J Rare Earth* 28 (2010) 742–746.

[90] C. Tang, J. Li, X. Yao, J. Sun, Y. Cao, L. Zhang, F. Gao, Y. Deng, L. Dong, "Mesoporous NiO–CeO2 catalysts for CO oxidation: Nickel content effect and mechanism aspect," *Appl Catal A* 494 (2015) 77-86.

[91] E. I. Papaioannou, D. Neagu, W. K. W. Ramli, J. T. S. Irvine, I. S. Metcalfe, "Sulfur-Tolerant, Exsolved Fe–Ni Alloy Nanoparticles for CO Oxidation," *Top Catal* (2018).

[92] Y. Li, Q. Fu, M. Flytzani-Stephanopoulos, "Low-temperature water-gas shift reaction over Cu- and Ni-loaded cerium oxide catalysts," *Appl Catal B* 27 (2000) 179-191.

[93] H. Yokokawa, T. Horita, N. Sakai, K. Yamaji, M. E. Brito, Y. P. Xiong, H. Kishimoto, "Ceria: Relation among thermodynamic, electronic hole and proton perperties," *Solid State Ionics* 177 (2006) 1705-1714.

[94] W. Y. Hernandez, M. A. Centeno, F. Romero-Sarria, J. A. Odriozola, "Synthesis and Characterization of Ce1-xEuxO2-x/2 Mixed Oxides and Their Catalytic Activities for CO Oxidation," *J Phys Chem C* 113 (2009) 5629-5635.

[95] M. Daturi, N. Bion, J. Saussey, J. C. Lavalley, C. Hedouin, T. Seguelong, G. Blanchard, "Evidence of a lacunar mechanism for activity in ceria-based deNOx catalysts," *Phys Chem Chem Phys* 3 (2001) 252-255.

[96] W. Y. Hernandez, O. H. Laguna, M. A. Centeno, J. A. Odriozola, "Structural and catalytic properties of lanthanide (La, Eu, Gd) doped ceria," *J Solid State Chem* 184 (2011) 3014-3020.

[97] X. Zhou, J. Ling, W. Sun, Z. Shen, "Fabrication of homogeneously Cu2+/La3+-doped CeO2 nanosheets and their application in CO Oxidation," *J Mater Chem A* 5 (2017) 9717-9722.

[98] P. Venkataswamy, D. Jampaiah, D. Mukherjee, C. U. Aniz, B. M. Reddy, "Mn-doped Ceria Solid Solutions for CO Oxidation at Lower Temperatures," *Catal Lett* 146 (2016) 2105-2118.

[99] Z. Huo, C. Chen, X. Liu, D. Chu, H. Li, Q. Peng, Y. Li, "One-pot synthesis of monodisperse CeO2 nanocrystals and superlattices," *Chem Commun* 32 (2008) 3741–3743.

[100] X. Liu, K. Zhou, L. Wang, B. Wang, Y. Li, "Oxygen Vacancy Clusters Promoting Reducibility and Activity of Ceria Nanorods," *J Am Chem Soc* 131 (2009) 3140–3141.

[101] C. Tang, Y. Bando, B. Liu, D. Golberg, "Cerium Oxide Nanotubes Prepared from Cerium Hydroxide Nanotubes," *Adv Mater* 17 (2005) 3005–3009.

[102] X. Liang, J. Xiao, B. Chen, Y. Li, "Catalytically Stable and Active CeO2 Mesoporous Spheres," *Inorg Chem* 49 (2010) 8188–8190.

[103] S. Wang, J. Zhang, J. Jiang, R. Liu, B. Zhu, M. Xu, Y. Wang, J. Cao, M. Li, Z. Yuan, S. Zhang, W. Huang, S. Wu, "Porous ceria hollow microspheres: Synthesis and characterization," *Microporous Mesoporous Mater* 123 (2009) 349–353.

[104] C. Y. Cao, Z. M. Cui, C. Q. Chen, W. G. Song, W. Cai, "Ceria Hollow Nanospheres Produced by a Template-Free Microwave-Assisted Hydrothermal Method for Heavy Metal Ion Removal and Catalysis," *J Phys Chem C* 114 (2010) 9865–9870.

[105] Y. Jiao, F. Wang, X. Ma, Q. Tang, K. Wang, Y. Guo, L. Yang, "Facile one-step synthesis of porous ceria hollow nanospheres for low temperature CO oxidation," Microporous Mesoporous Mater, 176 (2013) 1-7.

[106] R. J. Baxter, P. Hu, "Insight into why the Langmuir–Hinshelwood mechanism is generally preferred," *J Chem Phys* 116 (2002) 4379.

[107] G. Sedmak, S. Hocevar, J. Levec, "Kinetics of selective CO oxidation in excess of H2 over the nanostructured Cu0.1Ce0.9O2-y catalyst," 213 (2003) 135-150.

[108] G. Sedmak, S. Hocevar, J. Levec, "Transient kinetic model of CO oxidation over a nanostructured Cu0.1Ce0.9O2-y catalyst," 222 (2004) 87-99.

[109] C. Doornkamp, V. Ponec, "The universal character of the Mars and Van Krevelenmechanism," *J Molecular Catal A: Chem* 162 (2000) 19-32.

[110] A. P. Jia, S. Y. Jiang, J. Q. Lu, M. F. Luo, "Study of Catalytic Activity at the CuO-CeO2 Interface for CO Oxidation," *J Phys Chem C* 114 (2010) 21605-21610.

Chapter 3

EXPERIMENTAL DETAILS

3. 1 Synthesis of Ceria and Doped Ceria Nanofibers

To synthesize ceria nanofibers and doped ceria nanofibers, the electrospinning technique was used. Pure ceria nanofibers and six different doped ceria nanofibers were fabricated and for each doped sample, two different concentrations (10 mol%, 30 mol%) were used. Cerium nitrate hexahydrate ($Ce(NO_3)_3{\cdot}6H_2O$, Alfa Aesar), polyvinylpyrrolidone ($(C_6H_9NO)_n$, Alfa Aesar), and N', N-dimethylformamide ($HCON(CH_3)_2$, VWR LIFE SCIENCE) were used to produce template ceria nanofibers. Copper acetate monohydrate ($Cu(CO_2CH_3)_2{\cdot}H_2O$, SIGMA − ALDRICH), nickel nitrate hexahydrate ($Ni(NO_3)_2{\cdot}6H_2O$, Alfa Aesar), iron nitrate nonahydrate ($Fe(NO_3)_3{\cdot}9H_2O$, Alfa Aesar), cobalt nitrate hexahydrate ($Co(NO_3)_2{\cdot}6H_2O$, Alfa Aesar), manganese nitrate tetrahydrate ($Mn(NO_3)_2{\cdot}4H_2O$, Alfa Aesar), and lanthanum nitrate hexahydrate ($La(NO_3)_3{\cdot}6H_2O$, Alfa Aesar) were used as doping agents. Cerium nitrate hexahydrate and six different metal salts such as copper acetate monohydrate, nickel nitrate hexahydrate, iron nitrate nonahydrate, cobalt nitrate hexahydrate, manganese nitrate tetrahydrate, and lanthanum nitrate hexahydrate were used as received. Polyvinylpyrrolidone (PVP, MW 1,300,000) was used as the template polymer because it has an exceptionally large molecular weight and N', N-dimethylformamide (DMF) was used as the solvent. Solutions with 10 and 30 mol. % of metal dopants were prepared by dissolving appropriate amounts of metal salts and 1.93g cerium nitrate hexahydrate in 15mL of DMF. After dissolution is achieved after stirring at room temperature, 1.93g of PVP was added and stirred overnight to produce a viscous and homogeneous solution. The final solution was loaded in a BD 10 ml plastic syringe equipped with a stainless-steel blunt tip needle (21 gauges, 0.51-mm inner diameter). The syringe was

mounted horizontally and fastened to a syringe pump and the flow rate of the pump was set to 1.2 mL h^{-1}. The collecting plate was wrapped with aluminum foil and placed facing the syringe tip to collect the nanofibers. The distance between the needle tip and collector was fixed at 15 cm and the voltage supply was 18 kV, producing the 1.2 kV cm^{-1} electric field. With those electrospun conditions, the uniform fibrous structure was formed without droplets and/or beads. During the process, the humidity and temperature were maintained below 40 % and at roughly 293 K, respectively. The electrospun fibers were calcined at 873 K for 3 h with a heating rate of 1 K min^{-1} in the air to eliminate the polymer substance and obtain oxide nanofibers.

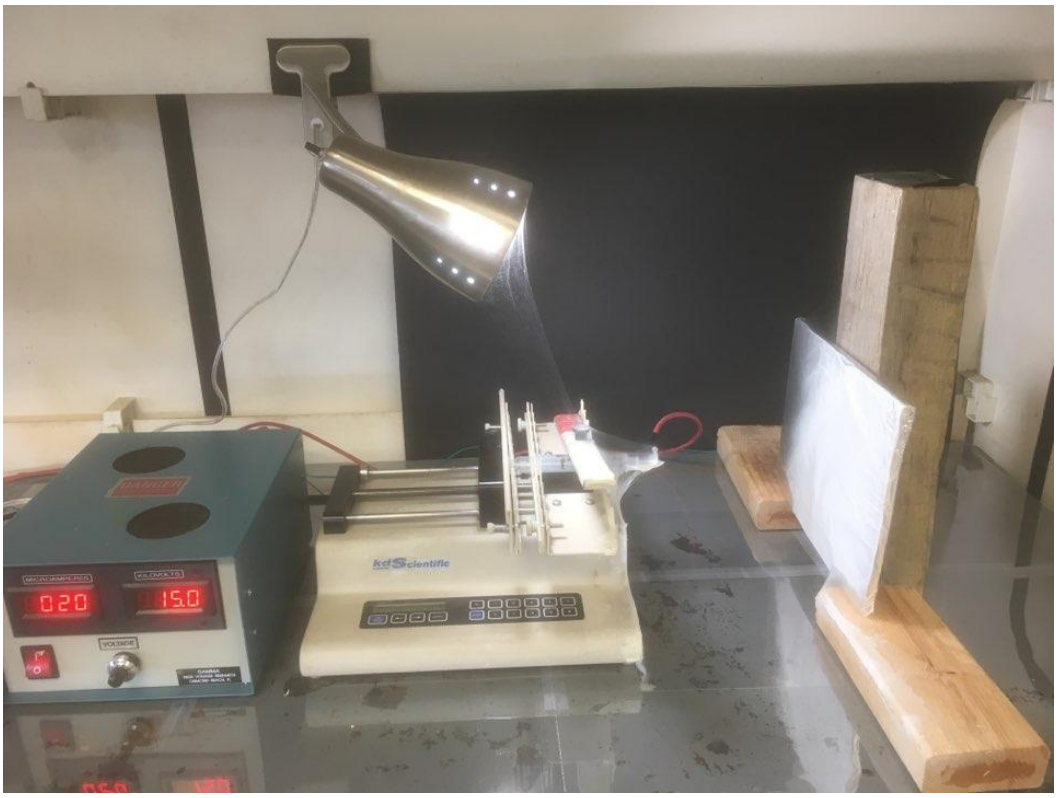

Figure 6. Electrospinning setup.

The electrospinning setup consists of a power supply, a syringe pump, a syringe tip, and a collector. There are anode and cathode from the power supply and the anode and cathode are connected to the syringe tip and collector respectively.

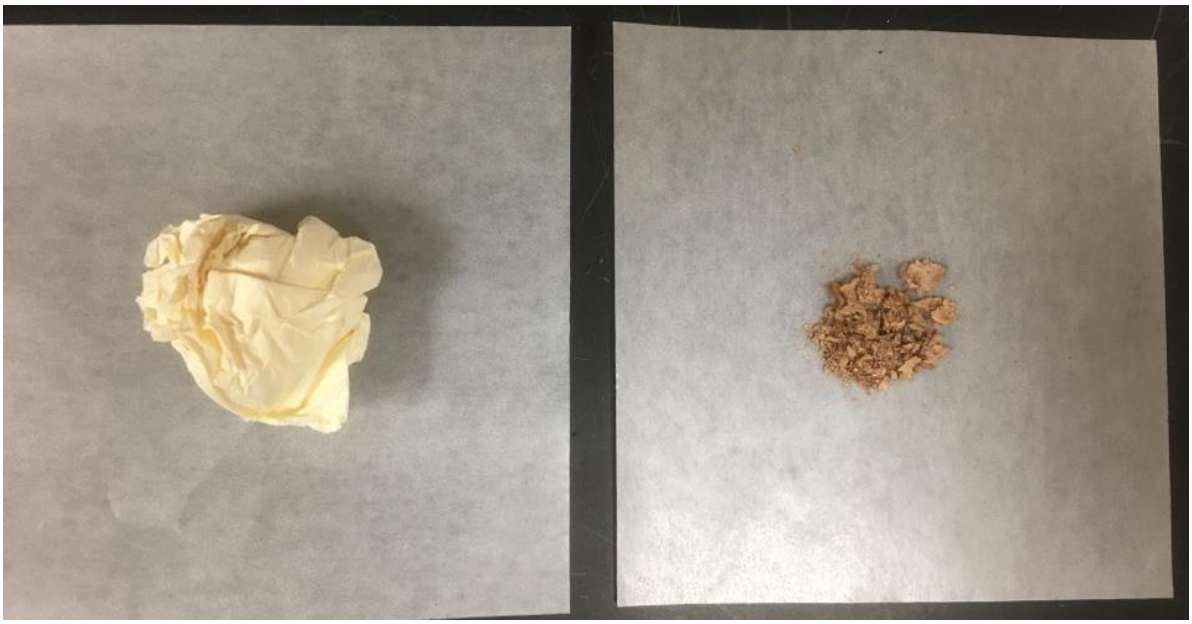

Figure 7. Before (left) and after (right) calcination of Fe-doped ceria fibers.

Figure 7 shows the electrospun fibers before and after calcination. Before calcination, the sample contains polymer template and salts, and after calcination, the sample is in a metal oxide form. After calcination, the sample is highly fragile and light, so for the purpose of using it as a catalyst, further handling is required. Press and mold in figure 8 were used to make it a pellet, so the sample can be loaded in a reactor easily.

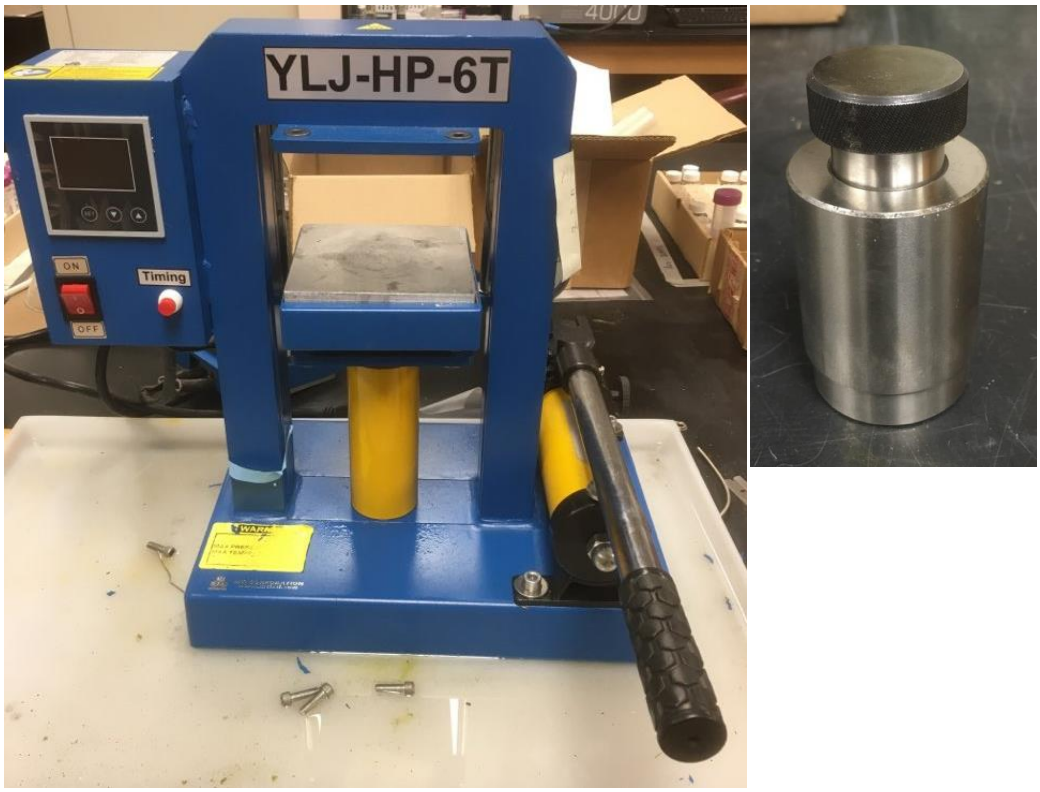

Figure 8. Press and mold for sample handling.

3. 2 CO Oxidation Experiment

Ceria particles and nanofibers were used as catalysts to measure catalytic activities for CO oxidation. For CO oxidation experiments, gas chromatography, two furnaces, two reactors, four gas tanks and three mass flow controllers (MFC) were used. The CO oxidation experiments were performed in a quartz tubular reactor (i.d. = 4 mm). A 200 mg of pressed catalysts were loaded in the reactor with the help of quartz wool. The flowing gases were 1% CO gas and 2% O_2 gas in nitrogen flow. The flow rates were maintained by three mass flow controllers and the overall flow was approximately 100 sccm (cm^3/min). The experiments were performed with different temperatures ranges from room temperature to 723 K in a fixed bed reactor at a ramp rate of 5 K min^{-1}. In every target temperature, the plateau was maintained for

30 minutes to reach a steady-state before gas analysis. The analysis was performed using the SRI 8610C gas chromatography equipped with a TCD detector.

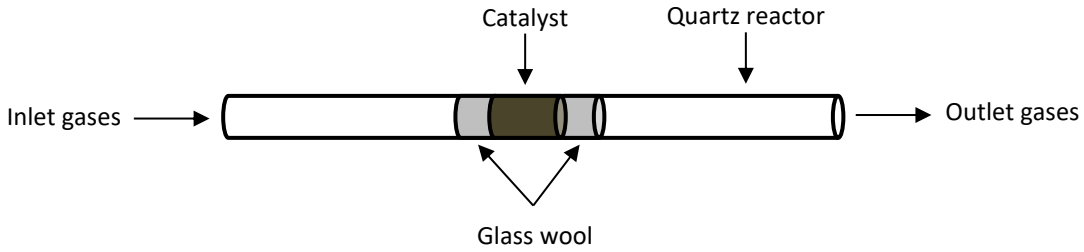

Figure 9. Packed bed reactor.

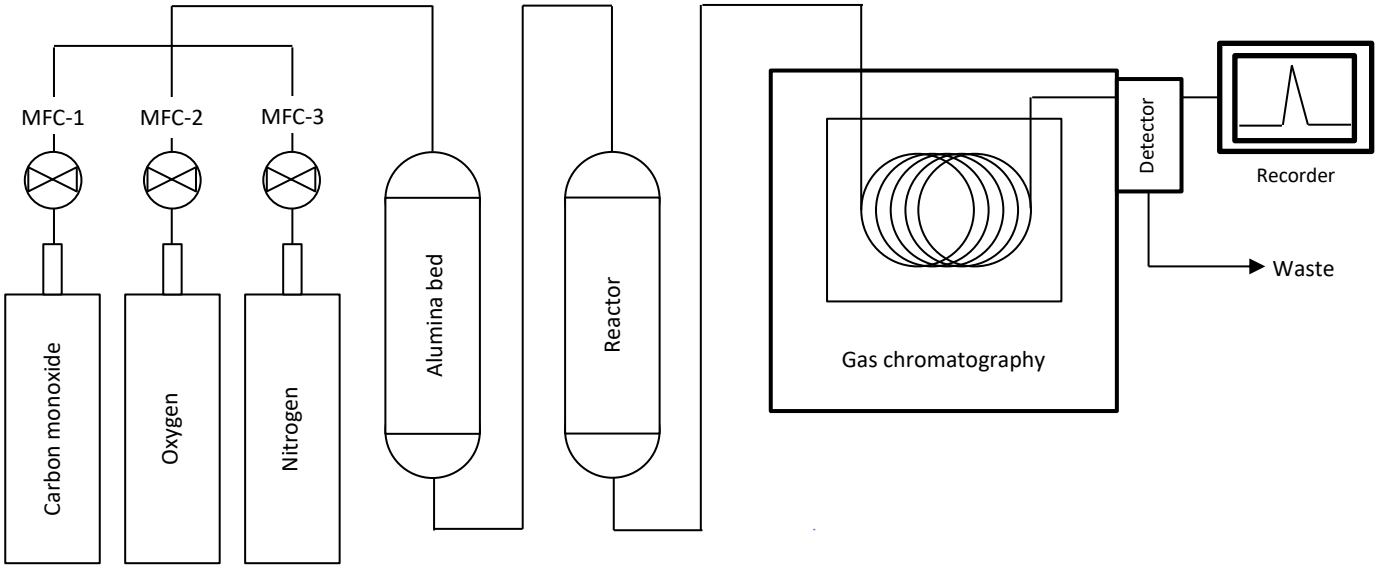

Figure 10. A schematic diagram of CO oxidation setup.

During the CO oxidation experiment, there were some difficulties with regard to the CO tank. The CO tank was producing iron carbonyl and giving it off through the pipes. It is well known that iron pentacarbonyl can form via gas-solid reactions under high pressure, like in a compressed gas cylinder [111].

$$Fe\ (s) + 5\ CO\ (g) \rightleftarrows Fe(CO)_5\ (l)$$

Not only iron pentacarbonyl easily formed under the conditions, but also, they are volatile complex. Therefore, the metal-containing impurities could be transferred in a gas phase and contaminating a device. It was checked by the color change of a catalyst in the reactor and the color of the catalyst turned to a reddish color. To prevent the contamination of the catalyst by the iron carbonyl, an alumina bed was installed before the reactor of the catalyst. 0.4g of alumina (Aluminum oxide, high surface area, Alfa Aesar) was ground to a fine powder form and loaded in a quartz tubular reactor. The alumina was widely spread in the reactor and the reactor was set to 400 ºC to effectively capture the iron carbonyl. The capture was successful, and it was proved by the color change of the alumina powder and no color change of the catalyst. The alumina was regularly disposed of and refilled before the color of alumina is completely changed. The image of iron carbonyl capture is given below.

Figure 11. Capture of iron carbonyl by alumina powder.

3. 3 Characterization of Ceria Particles and Nanofibers

Zeiss EVO50 scanning electron microscope (SEM) and Zeiss EM10 transmission electron microscope (TEM) were employed to study the morphology of the samples. The crystal structures of the catalysts were analyzed using the PROTO AXRD powder diffraction system (XRD). The X-ray was operated at 40 kV and 40 mA. TriStar II 3020 was employed to measure the BET surface area, and the nitrogen physisorption was performed at -196 ºC on samples previously degassed under vacuum to eliminate water and other contaminants. Raman spectroscopy (inVia, Renishaw) was used to analyze the structure of the catalysts. The instrument used 514.5 nm laser and the measurement range was 200 to 800 cm^{-1}.

Chapter 4

RESULTS AND DISCUSSIONS

4. 1 SEM and TEM Images of Ceria Nanofibers

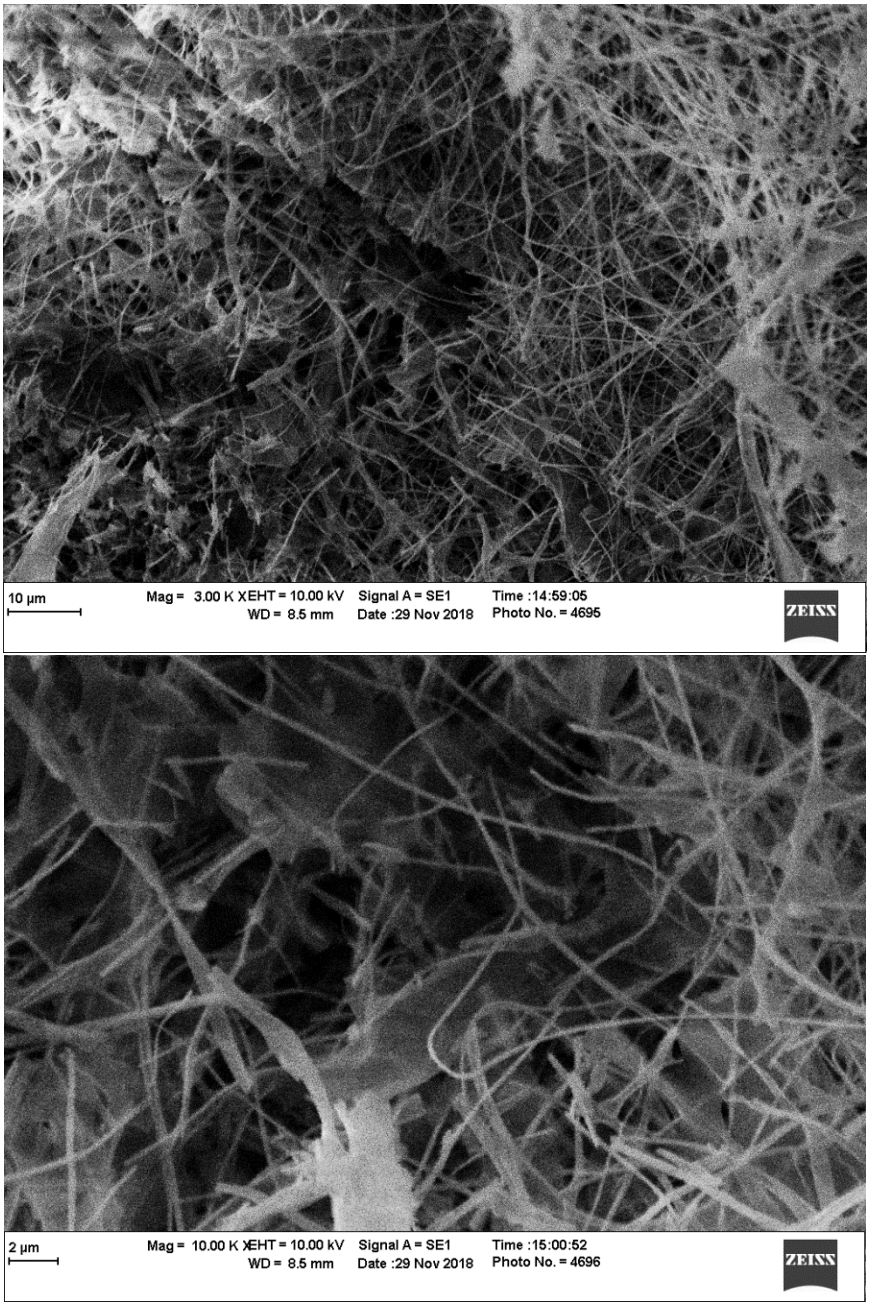

Figure 12. SEM images of ceria pure nanofibers.

Figure 13. TEM images of ceria nanofibers.

Figures 12 and 13 show the ceria nanofibers synthesized using the electrospinning technique. It shows a string like fibers with an average diameter of around 200 nm. The BET machine was used to measure the surface area of the fibers and the value was around 83 m^2/g. The catalytic activity of the ceria nanofibers was measured using the CO oxidation experiment and the result is shown below.

4. 2 Comparison of Ceria Nanofibers and Nanospheres

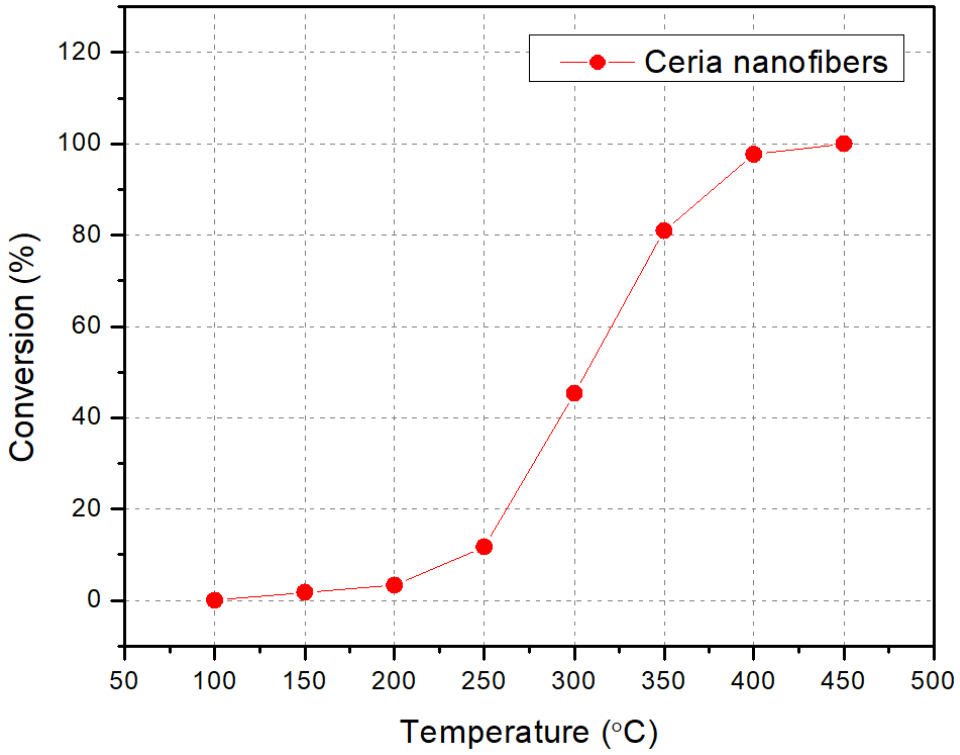

Figure 14. A CO oxidation graph of ceria nanofibers.

Figure 14 shows the CO oxidation graph, and the reaction started conversing CO to CO_2 from the temperature around 150 °C and the reaction reached the 100% conversion at the temperature around 450 °C.

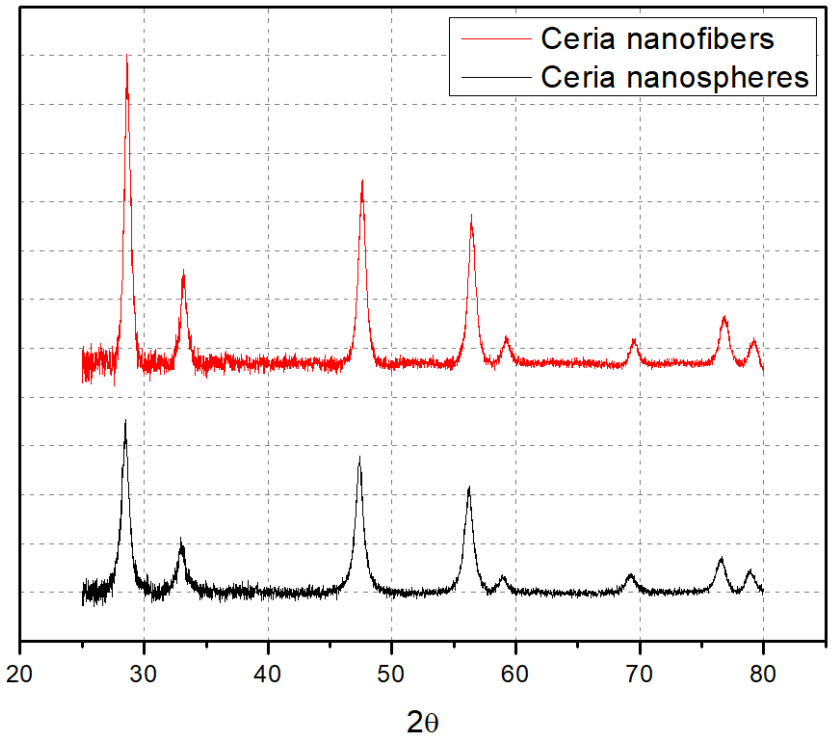

Figure 15. XRD patterns of ceria nanofibers and nanospheres.

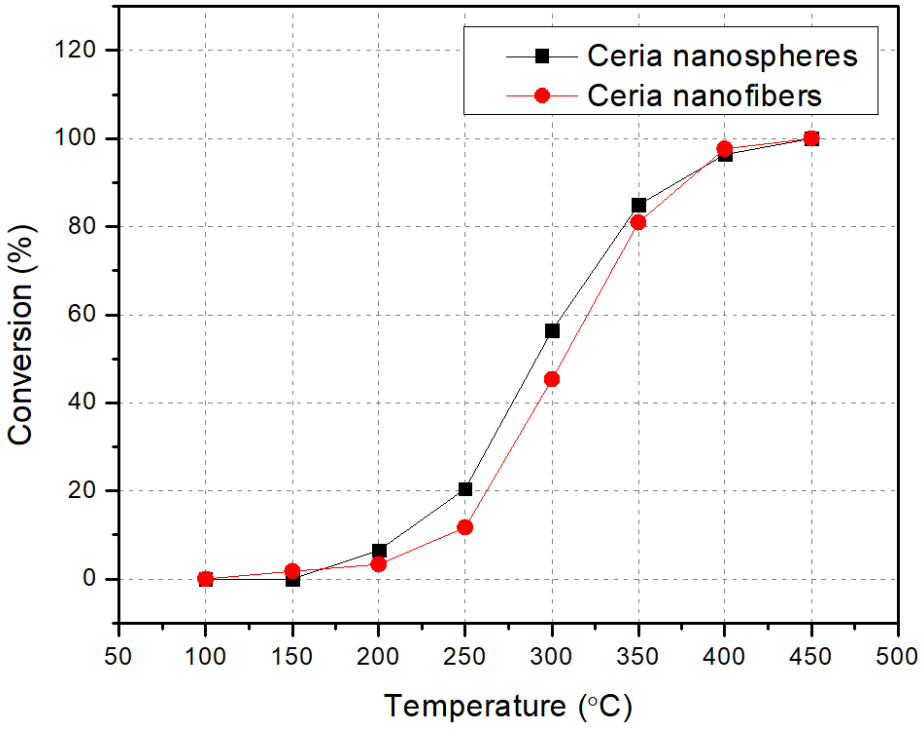

Figure 16. CO oxidation graphs of ceria nanospheres and nanofibers.

Figure 15 shows the XRD patterns of ceria nanospheres (Appendix) and nanofibers. Ceria nanofibers had higher crystallinity compared to the nanospheres, but it did not show better catalytic activity towards CO oxidation. As figure 16 shows, ceria nanospheres and nanofibers have quite similar CO conversion graphs. The result is consistent with the surface area since they have quite similar surface area values. It is commonly known that the higher the surface area is, the better the catalytic performance is. As the CO oxidation graphs and surface area values indicate, for ceria nanomaterials with different morphologies, catalytic performance could be related to the surface area.

4. 3 CO Oxidation Conversions of Doped Ceria Nanofibers

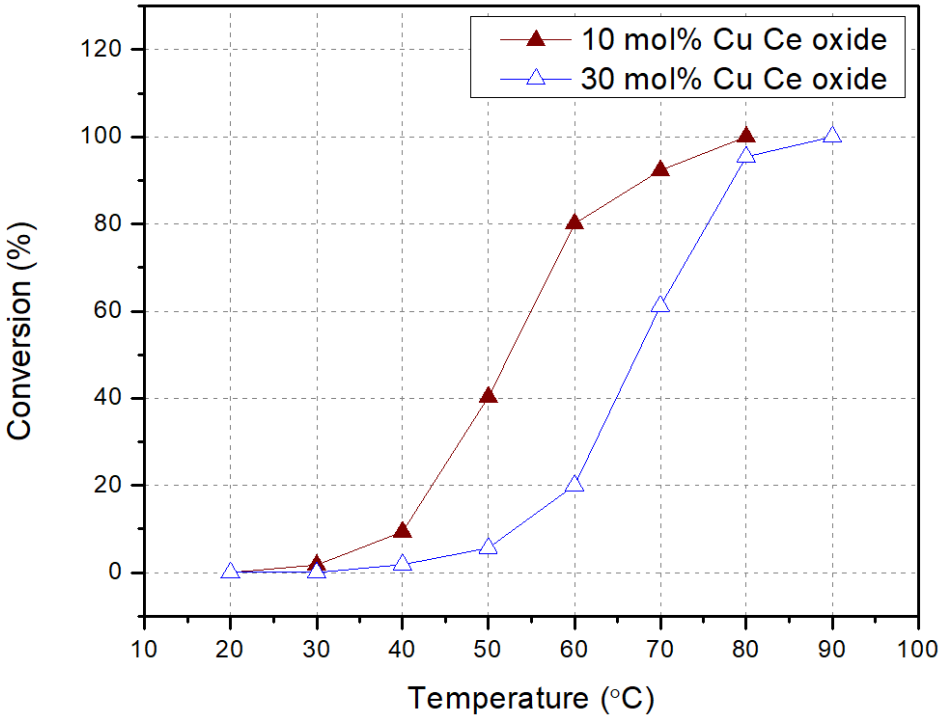

Figure 17. CO oxidation graphs of 10 and 30 mol% Cu-doped ceria.

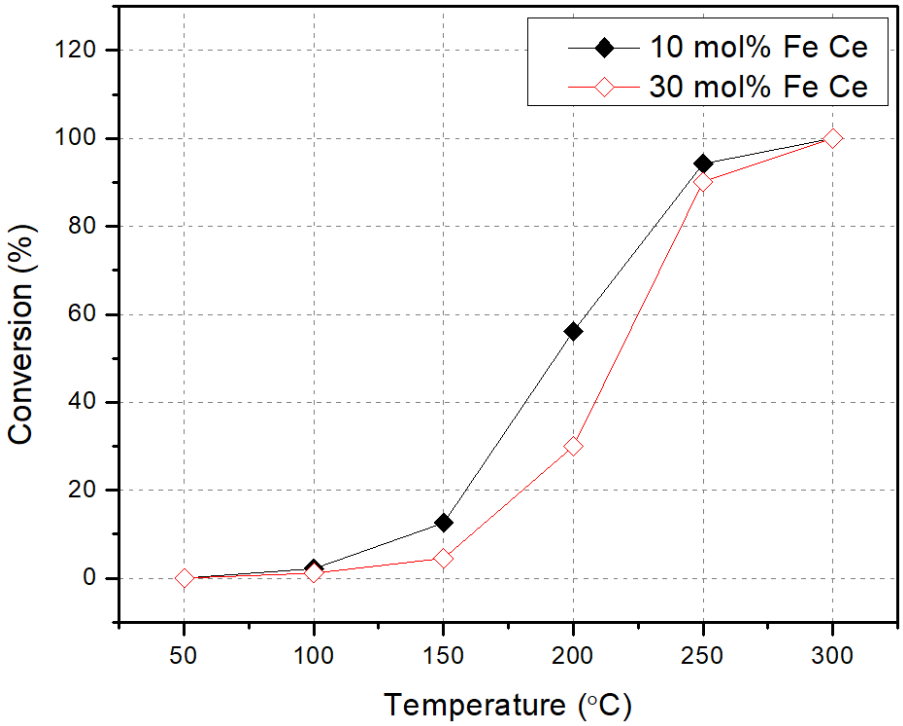

Figure 18. CO oxidation graphs of 10 and 30 mol% Fe-doped ceria.

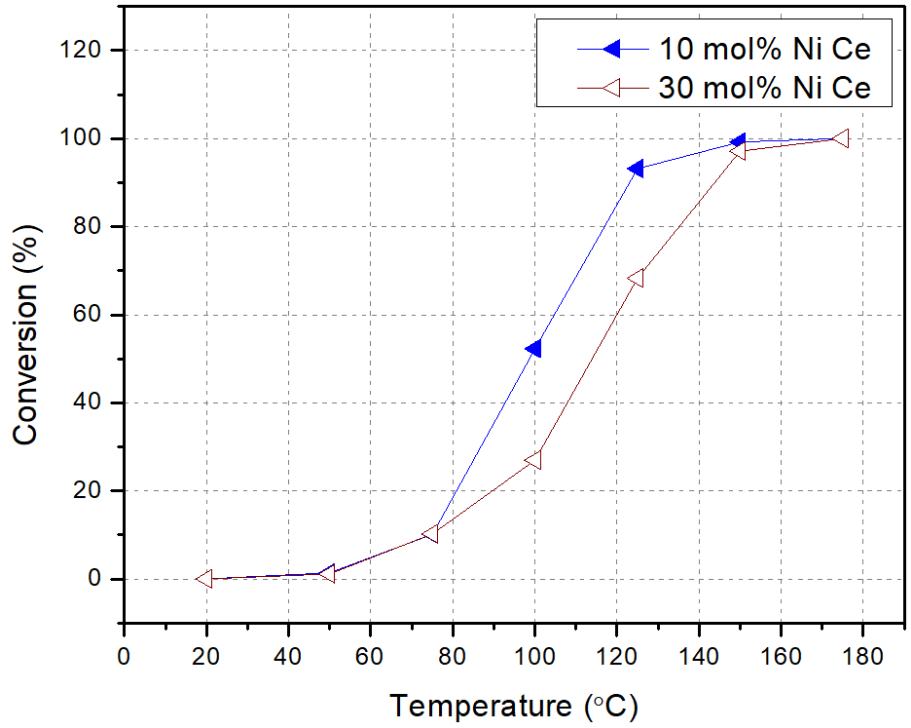

Figure 19. CO oxidation graphs of 10 and 30 mol% Ni-doped ceria.

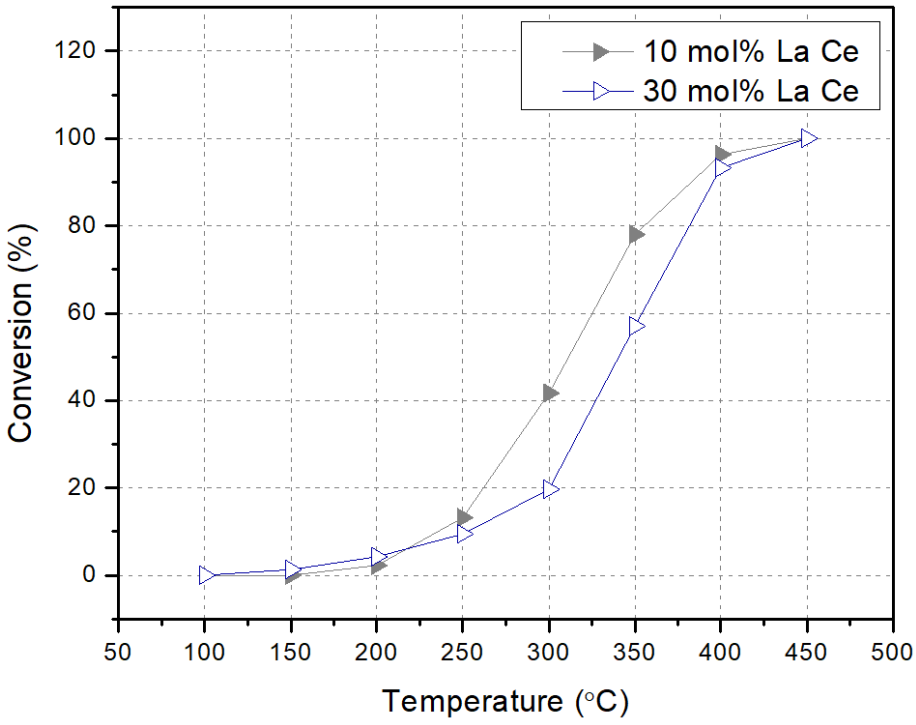

Figure 20. CO oxidation graphs of 10 and 30 mol% La-doped ceria.

Figures 17 to 20 show CO oxidation graphs of copper, iron, nickel, and lanthanum doped ceria with two different dopant contents (10 and 30 mol%). When ceria was doped with these four dopants, ceria with a lower amount of dopant had better catalytic activity. Based on the amount of dopant (10 and 30 mol%), they show similar temperatures for the completion of CO oxidation, however, they show quite big differences for the temperature of 50 % conversion. The ideal amount of dopant is not clear, but that could be found with further studies.

The improving effect of NiO on CO oxidation is apparent from the better activity of Ni-doped ceria nanofibers than ceria nanofibers alone. The enhanced catalytic activity of Ni-doped ceria nanofibers could be ascribed to the synergetic effect of NiO and ceria. Ni doping could enhance the amount of oxygen vacancies in the ceria lattice and enhances the migration of oxygen ions [112]. It was reported that doping Ni^{2+} and Zn^{2+} in ceria lattice was advantageous to lessen the formation energy of oxygen vacancy, thereby increasing the amount of oxygen vacancy and promoting CO oxidation activity [113, 114]. Also, NiO particles were reported to be active toward CO oxidation [115]. As the figure 19 shows, the catalytic activity of 10 mol% Ni-doped ceria is higher than 30 mol% Ni-doped ceria. Therefore, it is reasonable to believe that the increased amount of NiO on the ceria surface was not beneficial towards CO oxidation.

4. 4 Raman Spectra of Ceria and La-doped Ceria Nanofibers

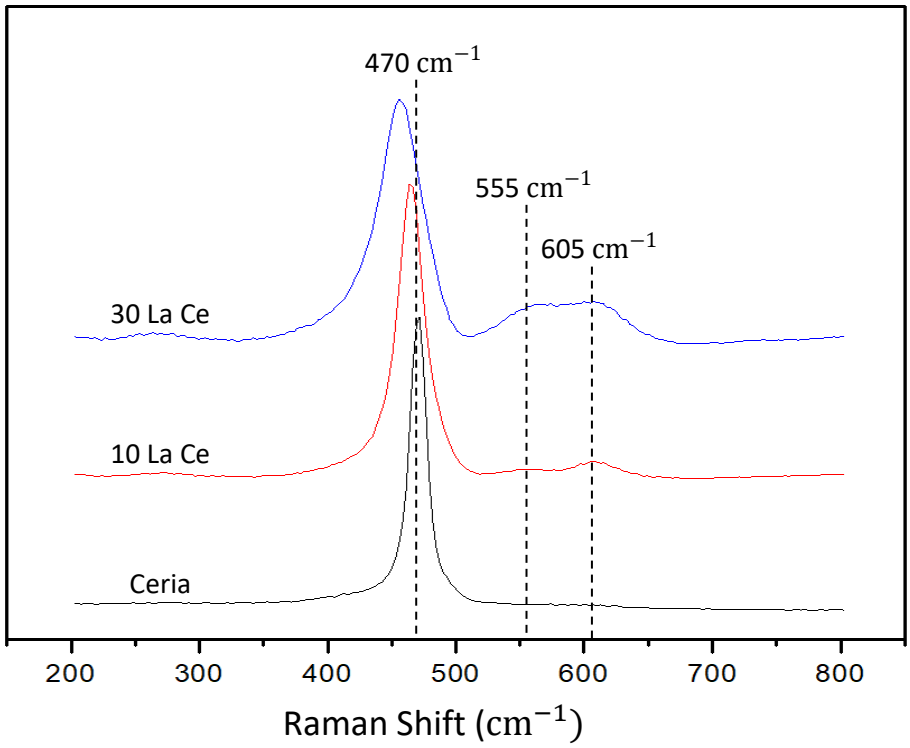

Figure 21. Raman spectra of ceria and 10 and 30 mol% La-doped ceria nanofibers.

Figure 21 shows the Raman spectra of 10 mol% and 30 mol% La-doped ceria nanofibers. The ceria sample shows a peak at around 470 cm^{-1} that is assigned to an F_{2g} vibration mode of the O atom surrounded by Ce cation, demonstrating the existence of fluorite-type structure [116]. Since the vibrational mode is only related to the movement of the oxygen atom, their peak characteristics (position and width) are highly affected by the dopant induced in the oxygen ion sublattice of the oxide [117, 118]. The peak of La-doped ceria samples shifts significantly towards lower wavenumbers with respect to the ceria sample, and the shift is more significant with the increasing amount of dopant. The shifting of the peak to lower wavenumbers demonstrates the formation of doped ceria solid solution and the incorporation of a dopant into

the ceria lattice decreases the Ce-O vibrational frequencies by the existence of a strong interaction between dopant and ceria [119]. The peak at around 555 cm^{-1} has been assigned to the extrinsic oxygen vacancies generated by the charge neutrality that is caused by the incorporation of the dopant into the ceria lattice [120, 121]. On the other hand, the peak at around 605 cm^{-1} has been assigned to the existence of intrinsic oxygen vacancies in ceria, because of their non-stoichiometric condition (Ce^{3+} replacing Ce^{4+} in the lattice) [120, 121].

Zhou et al. successfully synthesized Cu and La-doped ceria nanosheets using a one-step complexing coprecipitation (CC) method and used the catalysts for CO oxidation [122]. Interestingly, their CO oxidation result shows similarity to the result in this thesis. Their Cu-doped ceria sample had superior catalytic activity and the catalytic activity of the La-doped ceria sample was even worse than the ceria sample. However, Singhania Synthesized La-doped ceria nanoparticles and the sample had better CO oxidation activity than ceria [123]. Also, Hernandez et al. synthesized the La-doped ceria solid solution and the CO oxidation activity was better than the ceria sample [124]. From the result in this paper, the La-doped ceria sample (10 mol% and 30 mol%) had similar or worse CO oxidation activity than the ceria sample. The Raman result in figure 21 shows the spectrum of La-doped ceria samples and they had significant oxygen vacancy peaks and the peaks get bigger with the increasing amount of dopant. However, the 30 mol% La-doped ceria sample had the worst catalytic activity, so it is reasonable to believe that the already-existing oxygen vacancy is not the main factor that determines the CO oxidation activity of ceria-based catalysts.

4. 5 Comparison of Ceria, Cu-doped, and La-doped Ceria Nanofibers

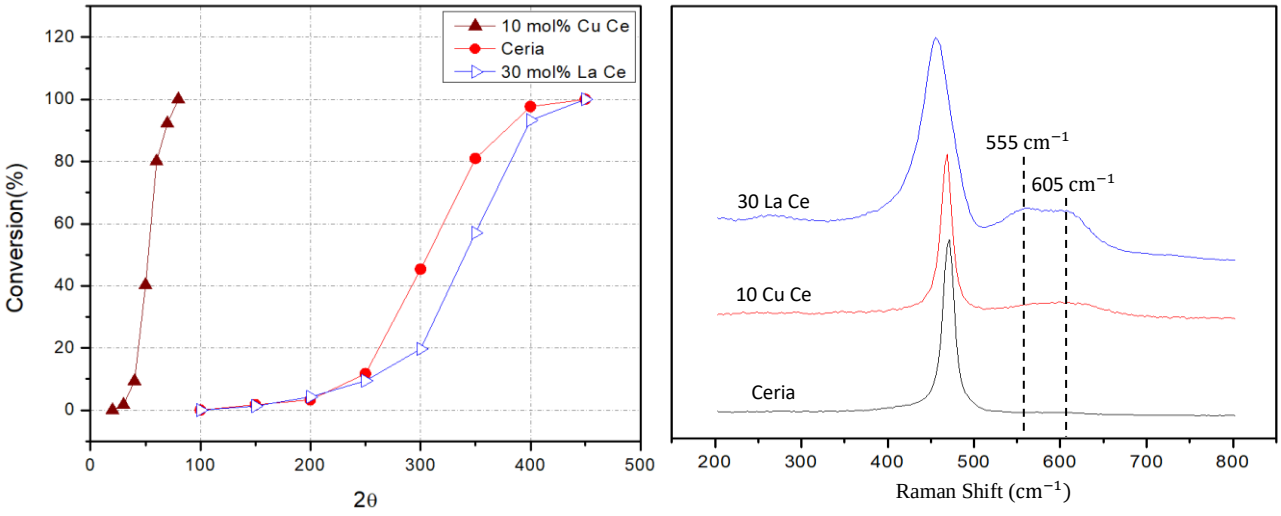

Figure 22. CO oxidation and Raman spectra of 10 mol% Cu-doped ceria, Ceria and 30 mol% La-doped ceria.

Figure 22 shows CO oxidation plots and Raman spectrum of 10 mol% Cu-doped ceria, ceria, 30 mol% La-doped Ce samples. Among all the doped ceria samples, 10 Cu Ce sample shows the best catalytic activity, and the 30 La Ce sample shows the worst catalytic activity. Interestingly, the 30 La Ce sample showed even worse catalytic activity than the ceria sample. However, as the Raman result shows, the 30 La Ce sample shows significant oxygen vacancy peaks, and that is even bigger than the ones of 10 Cu Ce sample. As discussed above, the oxygen vacancy is not the main factor that describes the CO oxidation activity of ceria-based catalysts. Also, the BET surface area can be used to explain the CO oxidation activity since the surface area is one of the influencing aspects of catalytic activity. It is commonly known that high surface area improves the contact area between active species and CO gas molecules and that increases the catalytic activity. The surface areas of 10 Cu Ce, ceria and 30 La Ce samples are 100, 83 and 90 m^2/g, respectively. The difference of the surface area values is not critical compared to the difference

of the catalytic activities, and the surface area of the ceria sample is even higher than the 30 La Ce sample. From the findings based on these samples, it is reasonable to believe that the dopants have bigger influences in CO oxidation activity compared to the concentration of oxygen vacancies and BET surface area values.

4. 6 XP Spectra of Fe-doped Ceria Nanofibers

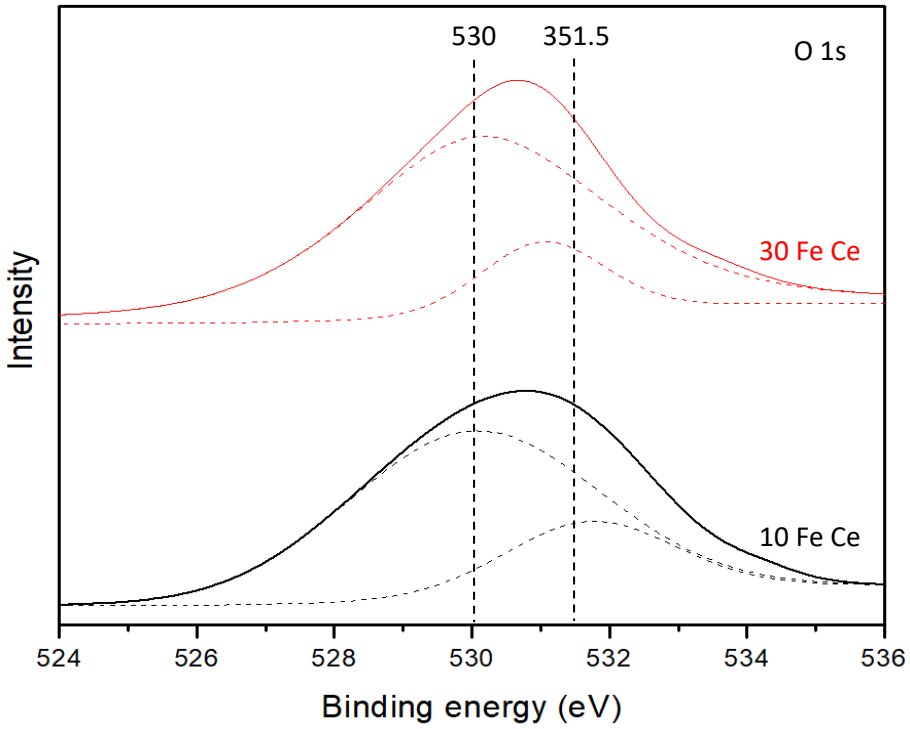

Figure 23. O 1s XP spectra of 10 and 30 mol% Fe-doped ceria nanofibers.

Figure 23 shows the O 1s XPS profiles of 10 and 30 mol% Fe-doped ceria nanofibers. The O 1s spectra are fitted into two peaks, suggesting the existence of different oxygen species. The peak at lower binding energy around 530 eV is assigned to the lattice oxygen and the peak at higher binding energy around 351.5 eV is assigned to the surface hydroxyl and carbonates species [125].

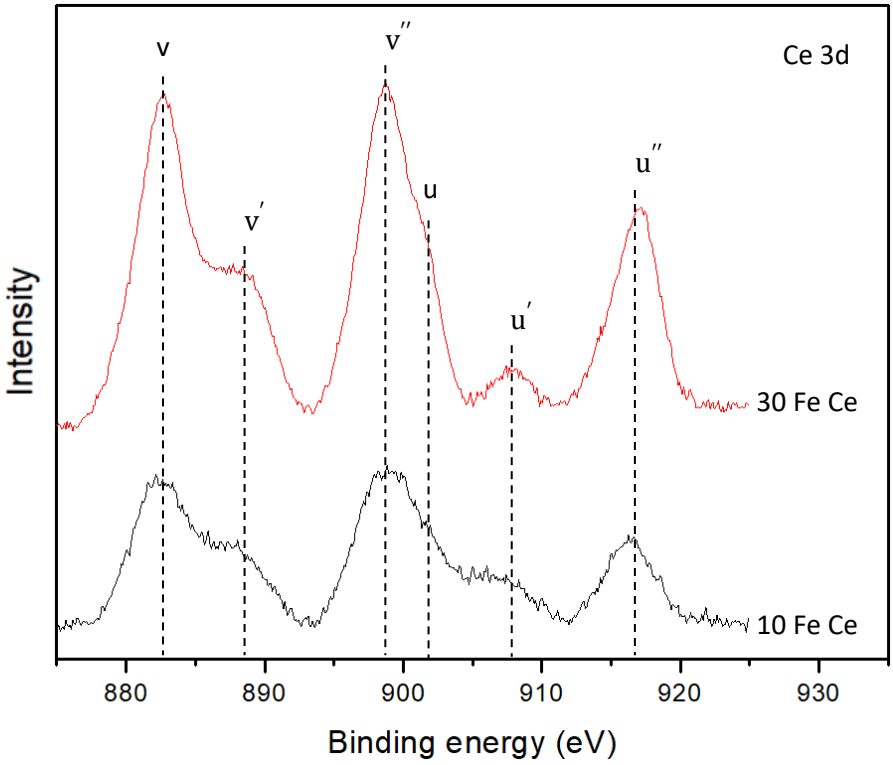

Figure 24. Ce 3d XP spectra of 10 and 30 mol% Fe-doped ceria nanofibers.

Figure 24 shows the Ce 3d XP spectra of 10 and 30 mol% Fe-doped ceria nanofibers. The labels in figure 24 follow the convention formed by Burroughs et al., in which v and u represent $3d_{3/2}$ and $3d_{5/2}$ spin-orbital components, respectively [126]. Among the peaks, the u'' peak is the most convenient feature to consider Ce reduction because it is only one peak that represents Ce^{4+} without overlapping. The intensity ratio of u'' peak to all Ce 3d peaks ($I_{u''}/I_{Total}$) is calculated to determine the surface composition of Ce^{3+} ions in a way that a smaller intensity ratio represents a higher Ce^{3+} concentration [109, 127]. The calculated $I_{u''}/I_{Total}$ values were 0.1432 and 0.1691 for 10 Fe Ce and 30 Fe Ce, respectively. Clearly, the less amount of dopant resulted in a higher concentration of Ce^{3+} ions in the ceria lattice, and the 10 mol% Fe-doped ceria sample had better catalytic activity as shown in figure 18. Perez-Alonso et al. reported that the presence of Ce^{3+} is a

direct result of the presence of the Fe-O-Ce bridges on the surface [74]. According to literature, charge compensation by incorporation of Fe will transform part of Ce^{4+} into Ce^{3+} associated with the formation of lattice defects and oxygen vacancies, which are positive for the oxygen mobility [127]. The XPS result well explains the surface chemistry of Fe-doped ceria samples, and when there were more Ce^{3+} ions in ceria lattice, the Fe-doped ceria sample had better catalytic activity towards CO oxidation.

BET surface areas of Cu and La-doped samples are measured, and the results are shown below.

Catalyst	Surface area (m^2/g)
10 mol% Cu Ce	100
30 mol% Cu Ce	51
10 mol% La Ce	93
30 mol% La Ce	90

Table 1. BET surface areas of Cu and La-doped ceria samples.

The surface area values of La-doped nanofibers are quite similar although 10 mol% La-doped ceria sample has a slightly higher surface area. The surface area of 30 mol% Cu-doped ceria significantly dropped compared to the 10 mol% Cu-doped ceria, and that could be because of the sintering of copper oxide particles during the high-temperature calcination. The surface area is one of the influencing aspects of CO oxidation. High surface area improves the contact area between active species and CO gas molecules which facilitate to increase the CO oxidation catalytic performance. Table 1 shows the higher surface areas of the 10 mol% doped ceria samples and they have better catalytic performances compared to the 30 mol% doped ceria

samples as figures 17 and 20 show. Therefore, it is reasonable to believe that the ceria nanofiber sample with the higher surface area has higher catalytic activity towards CO oxidation.

4. 7 CO Oxidation Conversions of Mn and Co-doped Ceria Nanofibers

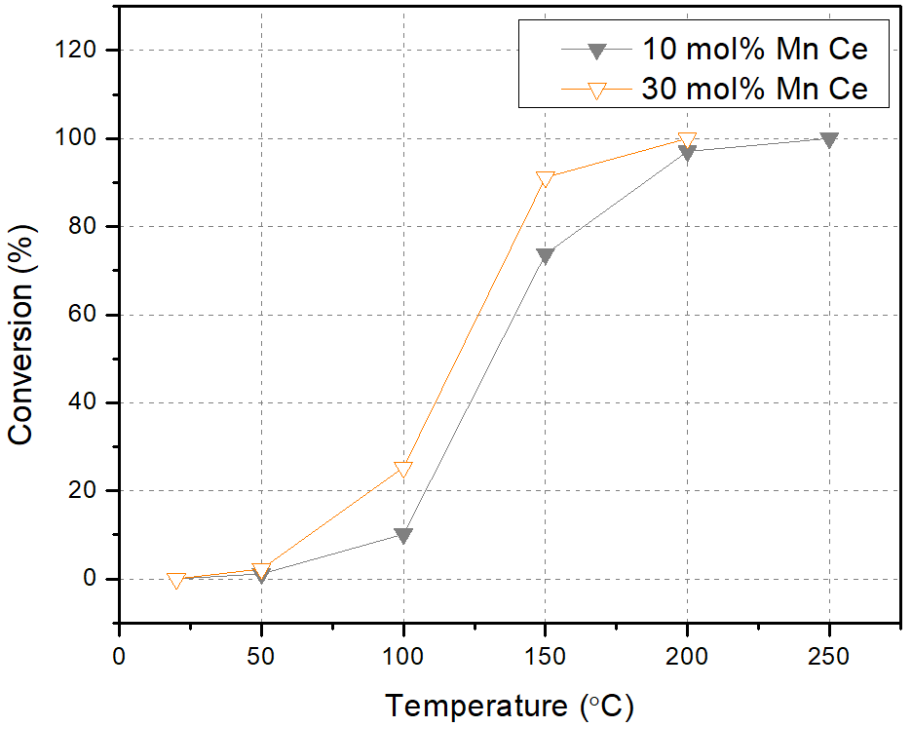

Figure 25. CO oxidation graphs of 10 and 30 mol% Mn-doped ceria.

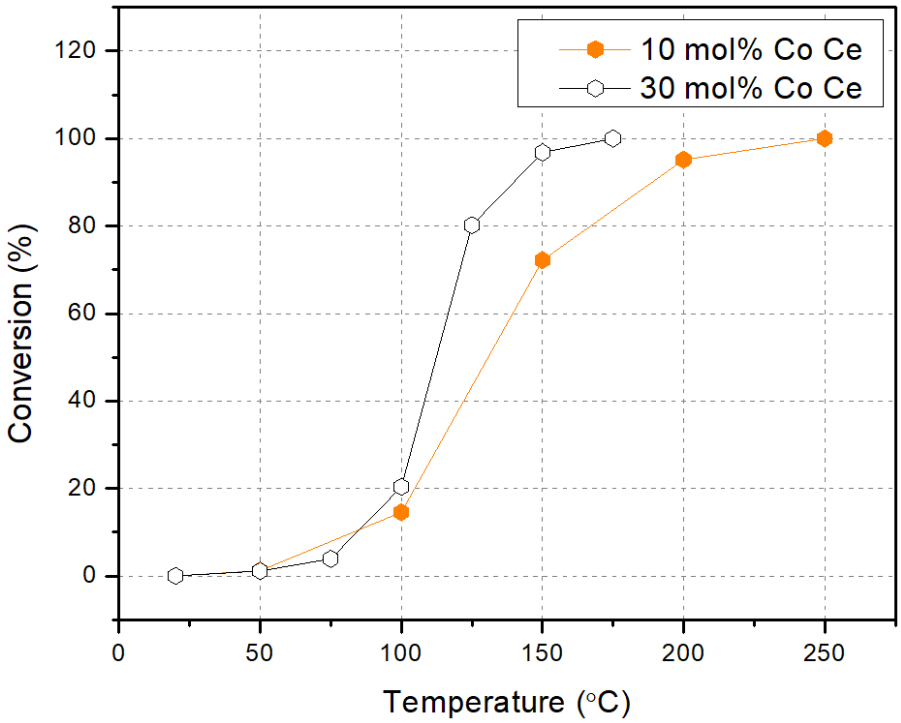

Figure 26. CO oxidation graphs of 10 and 30 mol% Co-doped ceria.

Figures 25 and 26 show CO oxidation graphs of manganese and copper doped ceria with two different dopant contents (10 and 30 mol%). When ceria was doped with these two dopants, ceria with a higher amount of dopant had better catalytic activity. They show quite big differences in catalytic activity, and further studied could be done to find the ideal amount of dopant.

4. 8 CO Oxidation Conversions and Temperatures of Complete Conversion

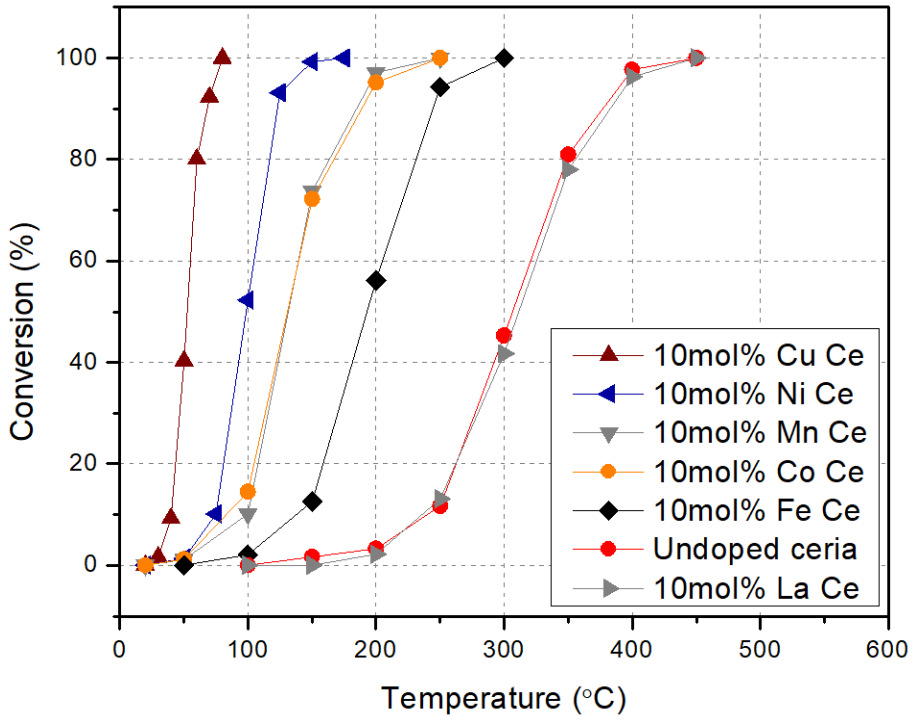

Figure 27. CO oxidation graphs of 10 mol% doped ceria samples.

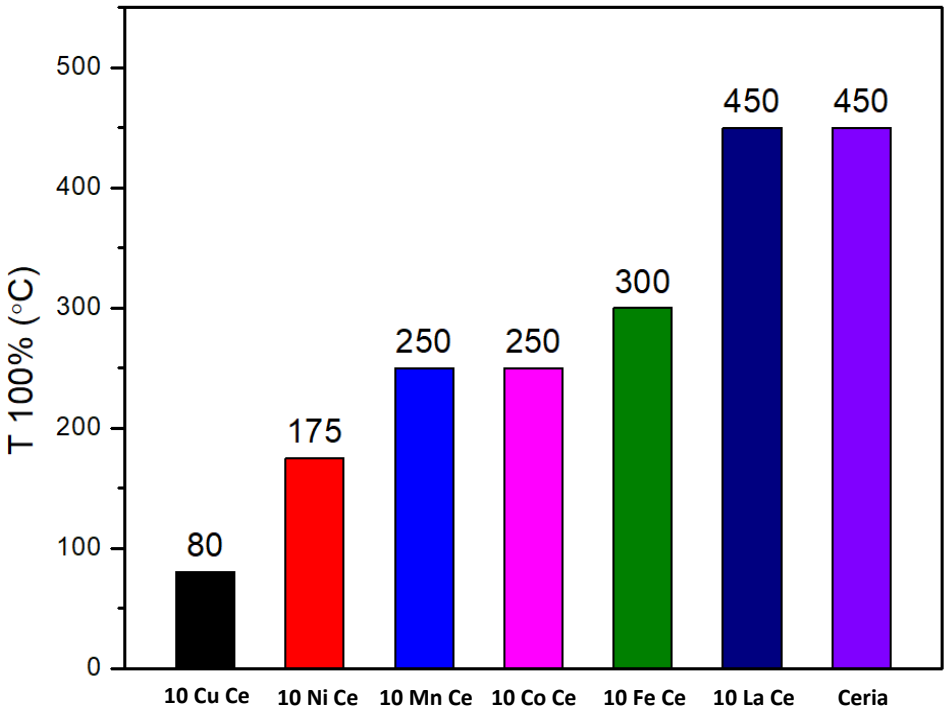

Figure 28. Temperatures of 100% CO conversion of the 10 mol% doped ceria samples.

Figure 27 shows the CO oxidation graphs of 10 mol% doped ceria catalysts. Cu-doped ceria shows the best catalytic activity, and La-doped ceria shows the worst catalytic activity. La-doped ceria's catalytic activity is almost the same with the catalytic activity of the undoped ceria sample, and that means La is not giving any benefit as a dopant. The catalytic activity order based on dopants is Cu, Ni, Mn, Co, Fe, and La, and Cu, Ni, Mn, Co, and Fe doping significantly increased the catalytic activity compared to the undoped ceria sample. Figure 28 shows the temperatures of 100% CO conversion using 10 mol% doped ceria catalysts. The result shows that there is a great increase in catalytic activity when the ceria nanofibers are doped with transition metals except for lanthanum.

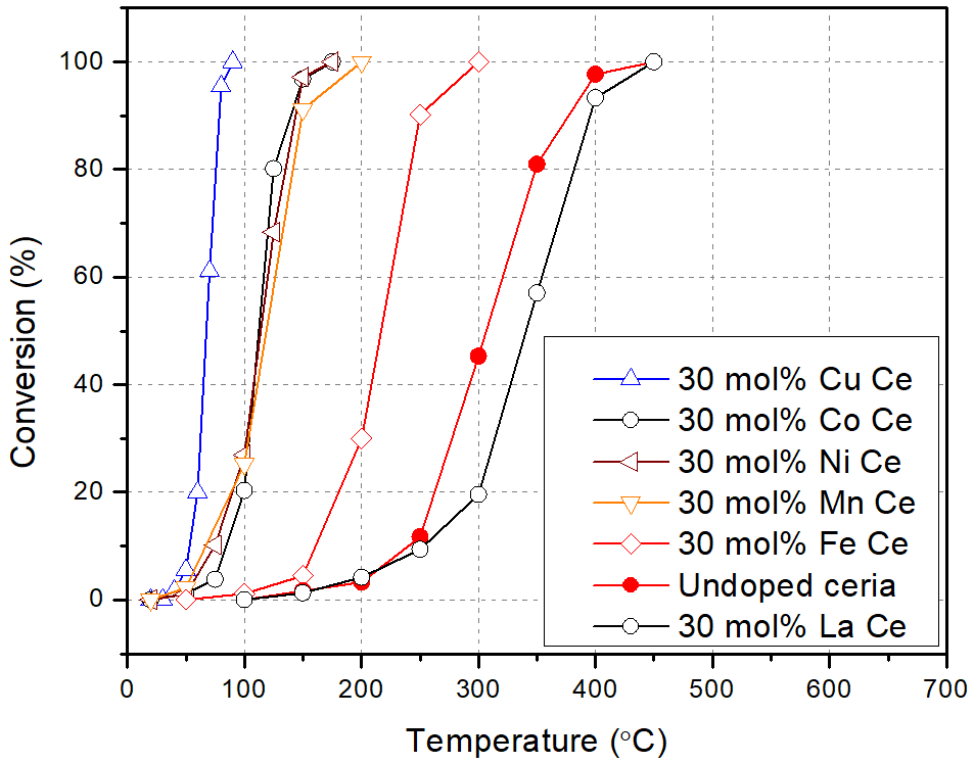

Figure 29. CO oxidation graphs of 30 mol% doped ceria samples.

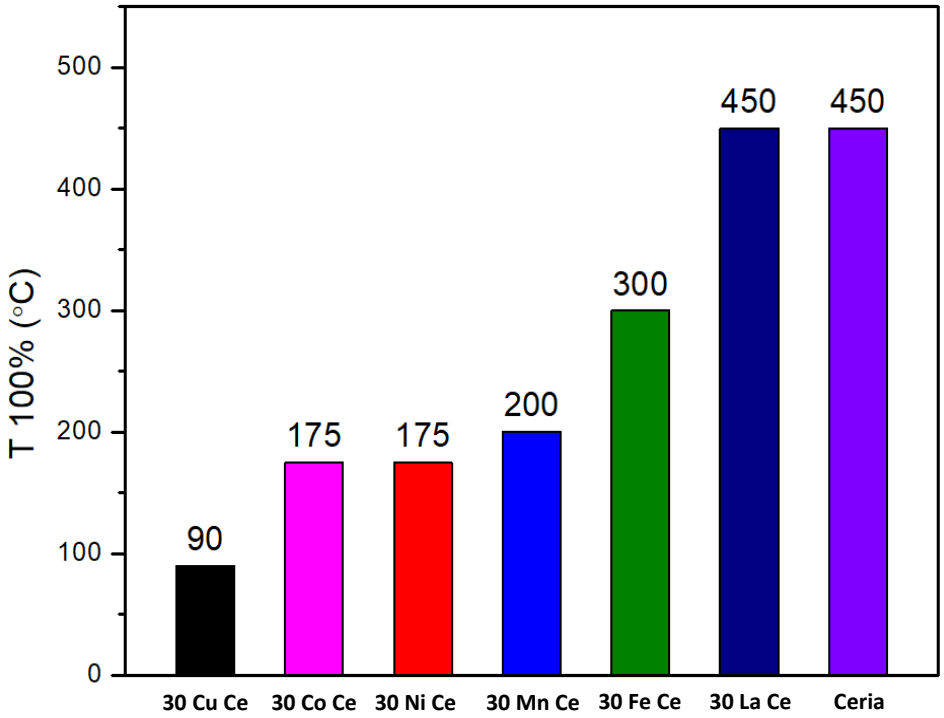

Figure 30. Temperatures of 100% CO conversion of the 30 mol% doped ceria samples.

Figure 29 shows the CO oxidation graphs of 30 mol% doped ceria samples. Cu-doped ceria shows the best catalytic activity, and La-doped ceria shows the worst catalytic activity. La-doped ceria's catalytic activity is even worse than the catalytic activity of the undoped ceria sample. Cu-doped ceria shows the best catalytic activity, and Cu, Co, Ni, Mn, and Fe doping significantly increased the catalytic activity compared to the undoped ceria sample. Figure 30 shows the temperatures of 100% CO conversion using 30 mol% doped ceria catalysts. The result shows that there is a great increase in catalytic activity when the ceria samples are doped with transition metals except for lanthanum.

The CO oxidation over Cu-doped ceria has been widely studied [58, 59]. It is well known that both the chemisorption of CO molecules on CuO species and the oxygen vacancies provided by the support are important for the reaction. The adsorption of oxygen on the surface of some

materials such as ceria results in the formation of O_2^- [128]. Bozo et al. suggested that the oxygen vacancies have an important role in the catalytic activity because they provide sites for oxygen activation by the formation of O_2^-, which is the intermediate species in the oxidation reactions occurring on the catalyst surface [129]. From CO oxidation results in this thesis, Cu-doped ceria has the best catalytic activity, which could be related to a higher concentration of oxygen vacancies in the sample. However, the above conclusion was achieved on the fresh catalyst, and the catalyst surface properties such as oxygen vacancies could change during the reaction due to the reducing agent CO in the gases. To study the change of catalyst after CO oxidation reaction, a fresh 10 mol% Cu Ce catalyst was used for CO oxidation reaction and after cooled down to room temperature, it was used again for CO oxidation. The CO oxidation and XRD results are shown below.

4. 9 CO Oxidation Conversions and XRD Data of 10 mol% Cu-doped Ceria Nanofibers

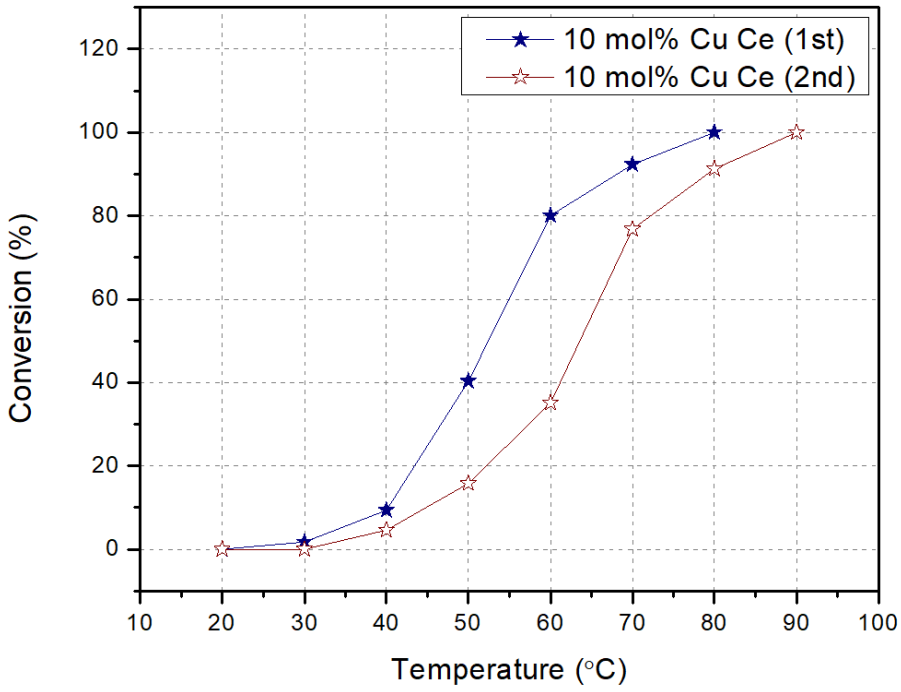

Figure 31. CO oxidation graphs of 10 mol% Cu Ce sample.

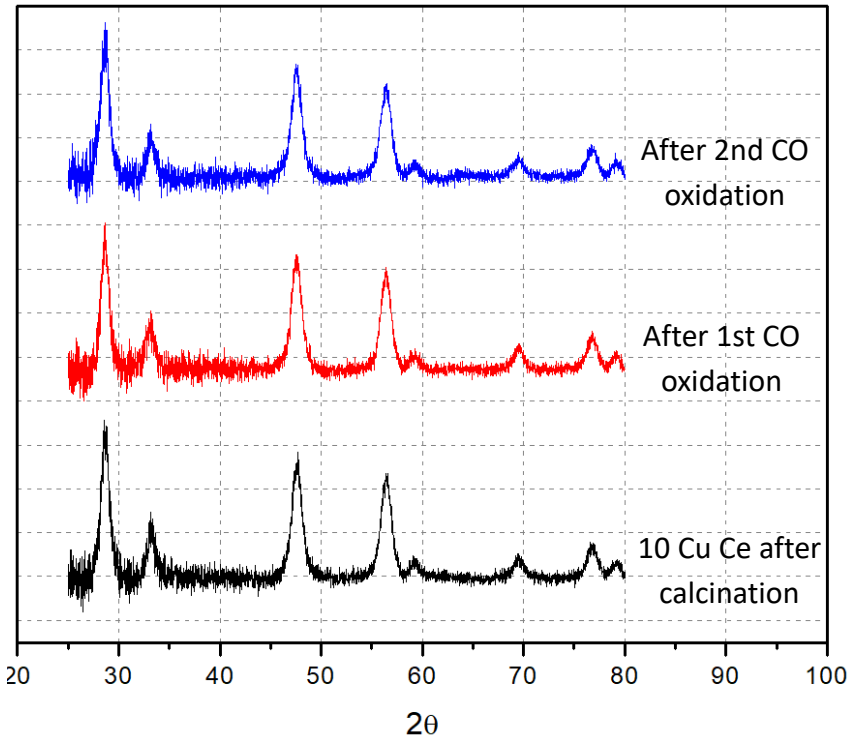

Figure 32. XRD patterns of 10 mol% Cu-doped ceria.

Figure 31 shows the CO oxidation graphs of 10 mol% Cu Ce catalyst. After the first CO oxidation experiment is done, the catalyst was cooled down to room temperature and then it was used again for CO oxidation. The 1st and 2nd in figure 31 mean the sequence of the experiments. The second time CO oxidation reaction showed lower catalytic activity and it could be proof of the discussion that the reducing agent CO could change the properties of the catalyst such as oxygen vacancies. Figure 32 shows the XRD patterns of 10 mol% Cu Ce catalyst, the sample after the first and second CO oxidation reaction. They show almost identical XRD patterns and that means the CO oxidation experiment does not change the crystallinity of the catalyst. To further investigate the surface information of the catalyst, in situ Raman experiments could be carried out.

The reaction process of Cu-doped ceria for CO oxidation reaction can be explained by that the CO and O_2 are chemisorbed on the Cu^+ and oxygen vacancies in the catalyst surface, respectively. And the chemisorbed O_2 is activated to O_2^- by oxygen vacancies, and the chemisorbed CO reacts with the activated O_2^- to form CO_2. Thus, ending the catalytic cycle by emptying the Cu^+ and oxygen vacancies [130].

4. 10 XRD Data of Nanofiber Samples

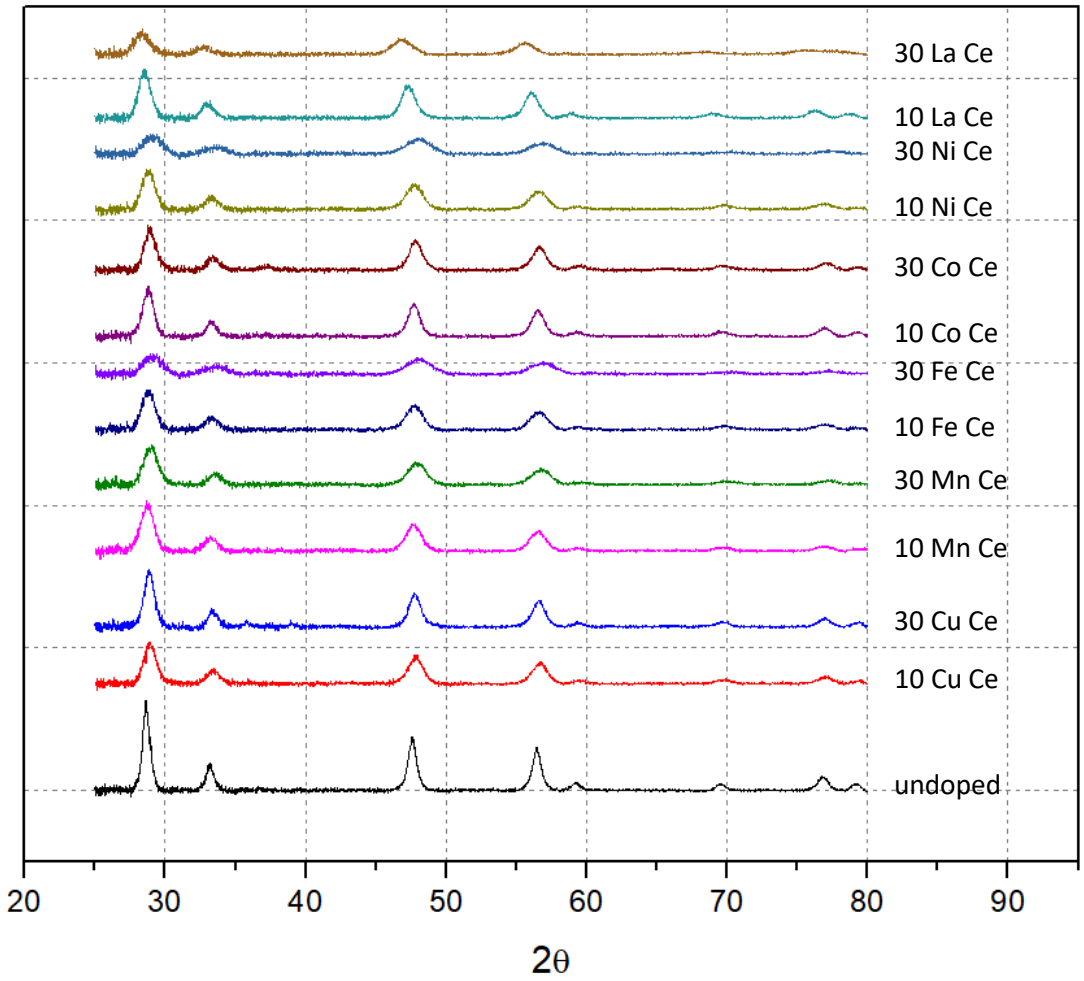

Figure 33. XRD patterns of ceria samples.

The structural property of the nanofiber samples was characterized by XRD and the results are shown in figure 33. It shows that the XRD patterns except for 30 mol% Cu Ce and 30 mol% Co Ce match the cubic ceria phase without any observed diffraction peaks due to the segregated phases of the dopants. That could be because the dopants are highly dispersed on the surface of ceria or the content of dopants was below the detection limit of XRD. By doping pure ceria nanofibers, the peak intensity of pure ceria is declined, suggesting a decline in ceria sizes occurs. The 30 mol% Cu and Co-doped ceria samples clearly show two phases of XRD patterns and that indicates the growth of CuO and Co_3O_4 crystallites (bulk CuO and Co_3O_4).

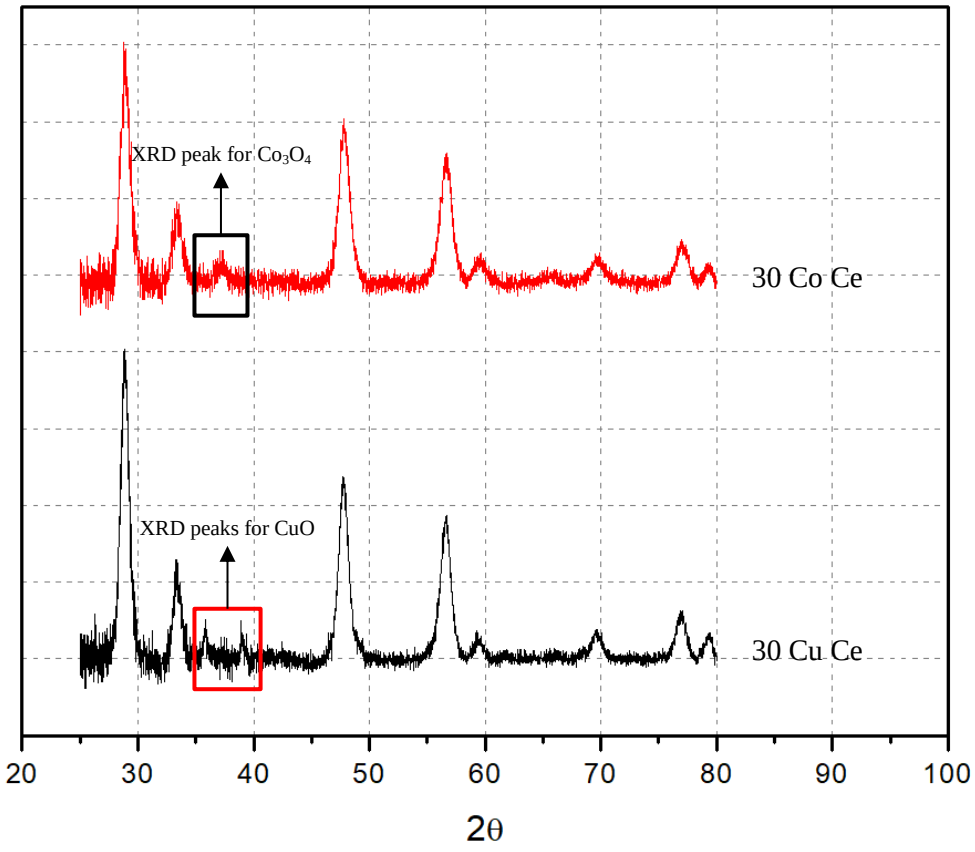

Figure 34. XRD patterns of 30 mol% Cu and Co-doped ceria samples.

Figure 34 shows the XRD patterns of 30 mol% Cu and Co-doped ceria samples and the rectangle marks indicate the weak XRD peaks for CuO and Co_3O_4 crystallites. The 30 mol% Cu-doped ceria sample shows two weak peaks at 35.5 and 38.7° because of the monoclinic CuO phase and 30 mol% Co-doped ceria sample shows a weak peak at 36.88° indicating the cubic Co_3O_4 phase. 30 mol% Cu and Co-doped ceria samples show two phases of XRD patterns and that means bulk CuO and Co_3O_4 are formed on the surface of ceria lattice. Since the 30 mol% Cu-doped ceria sample shows worse catalytic performance compared to the 10 mol% Cu-doped ceria sample, it is reasonable to believe that the high bulk copper oxide was not increasing the catalytic performance. On the contrary, 30 mol% Co-doped ceria sample shows better catalytic performance compared to 10 mol% Co-doped ceria sample. 30 mol% Co-doped ceria sample showed better catalytic performance and that indicates the bulk Co_3O_4 on the ceria surface produce some specific sites that increase the adsorption of gas molecules and promote the catalytic performance. Lin et al. found out that Co_3O_4 had better catalytic performance than CoO_x towards CO oxidation because the lattice oxygen on Co_3O_4 is more active for CO oxidation [131]. Therefore, it is reasonable to believe that the bulk Co_3O_4 on the ceria lattice is helping to increase the catalytic performance towards CO oxidation.

4. 11 Crystallite Sizes and Lattice Parameters of Nanofiber Samples

Catalyst (nanofibers)	Crystallite size (nm)	Lattice parameter (Å)
Ceria	13.64	5.403
10 mol% Cu Ce	8.36	5.388
30 mol% Cu Ce	10.18	5.392
10 mol% Ni Ce	8.07	5.393
30 mol% Ni Ce	5.21	5.364
10 mol% Mn Ce	7.99	5.394
30 mol% Mn Ce	7.16	5.371
10 mol% Co Ce	9.94	5.395
30 mol% Co Ce	9.44	5.388
10 mol% Fe Ce	8.05	5.392
30 mol% Fe Ce	5.20	5.365
10 mol% La Ce	8.98	5.434
30 mol% La Ce	6.44	5.479

Table 2. Crystallite sizes and lattice parameters of ceria samples.

The crystallite sizes were calculated by the Scherrer equation using the full width at half maximum (FWHM) values of the (111) lattice plane and the values are shown in table 2. From the results in table 2, all the dopants decreased the crystallite size of the pure ceria sample. There was no relation between the crystallinity of doped ceria and CO oxidation because the Cu-doped ceria sample has similar crystallite size to La-doped ceria even though the Cu-doped ceria sample has superior catalytic activity.

The lattice parameters of all samples were calculated and given in table 2. Lattice parameters of doped ceria nanofibers were decreased compared to pure ceria nanofibers (5.403 Å) except for

the La-doped ceria nanofibers. When the ceria nanofibers were doped with lanthanum, the lattice parameters were increased (10 mol% La Ce - 5.434, 30 mol% La Ce - 5.479 Å). The change of lattice parameters could be explained by the substitution of the smaller (Cu, Ni, Mn, Co, and Fe) or bigger ion (La) for the cerium ion, thereby the incorporation of the ion into the ceria lattice.

Chapter 5

CONCLUSION

In summary, we have prepared undoped ceria particles using microwave-assisted and hydrothermal methods. Using the microwave-assisted method, random-shaped ceria particles were synthesized and using the hydrothermal method, ceria nanospheres with an average diameter of around 200 nm were successfully synthesized. The nanosphere sample was characterized using XRD and BET machine and used to measure catalytic activity of CO oxidation. The undoped and transition-metal doped ceria nanofibers were successfully synthesized using the electrospinning technique and 6 different dopants (Cu, Co, Mn, Ni, Fe, and La) were used with two different concentrations (10 and 30 mol%). The pure metal oxide solids were obtained by calcination at 600 ºC and the nanofiber samples were characterized using XRD, Raman, XPS, and BET machine. Also, the nanofiber samples were used to measure catalytic activities of CO oxidation.

The undoped ceria nanosphere and nanofiber samples had similar catalytic activities toward CO oxidation and that could be explained by the similar surface area values. The doped ceria nanofiber samples had different catalytic activities toward CO oxidation based on the dopants. Especially from the La-doped nanofiber samples, the surface area and the concentration of oxygen vacancies were measured. Based on the results, the sample with high surface area and lower oxygen vacancies had better CO oxidation activity. From the 10 mol% Cu and 30 mol% La-doped nanofiber samples, surface area and the concentration of oxygen vacancies were measured. Based on the results, the Cu-doped sample had a lot better CO oxidation activity regardless of the lower oxygen vacancy concentrations and similar surface area values.

Therefore, we could conclude that the dopants have bigger influences in CO oxidation activities than the BET surface area and the concentration of oxygen vacancies. We speculate that the adsorption of CO onto the dopants is the key factor to explain the CO oxidation activity of the doped ceria-based nanocatalysts.

5. 1 References

[111] C. Wyse, T. Watanabe, J. Vininski, R. Torres, M. Raynor, V. Houlding, "Contamination Control in Carbon Monoxide Processes," matheson gas.

[112] S. T. Aruna, K. C. Patil, "COMBUSTION SYNTHESIS AND PROPERTIES OF NANOSTRUCTURED CERIA-ZIRCONIA SOLID SOLUTIONS," *Nanostruct Mater* 10 (1998) 955–964.

[113] M. Nolan, "Enhanced oxygen vacancy formation in ceria (111) and (110) surfaces doped with divalent cations," J Mater Chem 21 (2011) 9160–9168.

[114] A. B. Kehoe, D. O. Scanlon, G. W. Watson, "Role of Lattice Distortions in the Oxygen Storage Capacity of Divalently Doped CeO2," *Chem Mater* 23 (2011) 4464–4468.

[115] D. Wang, R. Xu, X. Wang, Y. Li, "NiO nanorings and their unexpected catalytic property for CO oxidation," *Nanotechnology* 17 (2006) 979–983.

[116] A. B. Lopez, I. S. Basanez, C. S-M. D. Lecea, " Stabilization of active Rh2O3species for catalytic decompositionof N2O on La-, Pr-doped CeO2," *J Catal* 244 (2006) 102-112.

[117] V. G. Keramidas, W. B. White, "Raman spectra of oxides with the fluorite structure," *J Chem Phys* 59 (1973) 1561.

[118] I. Kosacki, V. Petrovsky, H. U. Anderson, P. Colomban, "Raman Spectroscopy of Nanocrystalline Ceria and Zirconia Thin Films," J Am Ceram Soc 85 (2002) 2646-50.

[119] I. Kosacki, T. Suzuki, H. U. Anderson, P. Colomban, "Raman scattering and lattice defects in nanocrystallineCeO2thin films," *Solid State Ionics* 149 (2002) 99-105.

[120] J. R. McBride, K. C. Hass, B. D. Poindexter, W. H. Weber, "Raman and x-ray studies of Ce1−xRExO2−y, where RE=La, Pr, Nd, Eu, Gd, and Tb," *J Appl Phys* 76 (1994) 2435.

[121] Z. D. Dohcevic-Mitrovic, M. Radovic, M. Scepanovic, M. Grujic-Brojcin, Z. V. Popovic, "Temperature-dependent Raman study of Ce0.75Nd0.25O2-y nanocrystals," Appl Phys Lett 91 (2007) 203118.

[122] X. Zhou, J. Ling, W. Sun, Z. Shen, "Fabrication of homogeneously Cu2+/La3+-doped CeO2 nanosheets and their application in CO Oxidation," *J Mater Chem A* 5 (2017) 9717-9722.

[123] A. Singhania, "High Surface Area M (M = La, Pr, Nd, and Pm)-Doped Ceria Nanoparticles: Synthesis, Characterization, and Activity Comparison for CO Oxidation," *Ind Eng Chem Res* 56 (2017) 13594-13601.

[124] W. Y. Hernandez, O. H. Laguna, M. A. Centeno, J. A. Odriozola, "Structural and catalytic properties of lanthanide (La, Eu, Gd) doped ceria," J Solid State Chem 184 (2011) 3014-3020.

[125] T. F. Moulder, W. F. Stickle, P. E. Sobol, K. D. Bomben, "Handbook of X-ray photoelectron spectroscopy," (1992) Perkin Elmer, Eden Prairie, Minnesota

[126] P. Burroughs, A. Hamnett, A. F. Orchard, G. Thornton, "Satellite Structure in theX-Ray Photoelectron Spectra of some Binary and Mixed Oxides of Lanthanum and Cerium," *J Chem Soc Dalton Trans* (1976) 1686-1698.

[127] M. Shen, J. Wang, J. Shang, Y. An, J. Wang, W. Wang, "Modification Ceria-Zirconia Mixed Oxides by Doping Sr Using the Reversed Microemulsion for Improved Pd-Only Three-Way Catalytic Performance," *J Phys Chem C* 58 (2011) 259-268.

[128] X. Zhang, K. J. Klabunde, "Superoxide (02-) on the Surface of Heat-Treated Ceria. Intermediates in the Reversible Oxygen to Oxide Transformation," *Chem* 31 (1992) 1706-1709.

[129] C. Bozo, N. Guilhaume, J. M. Herrmann, "Role of the Ceria–Zirconia Support in the Reactivity of Platinum and Palladium Catalysts for Methane Total Oxidation under Lean Conditions," *J Catal* 203 (2001) 393-406.

[130] Z. Y. Pu, X. S. Liu, A. P. Jia, Y. L. Xie, J. Q. Lu, M. F. Luo, "Enhanced Activity for CO Oxidation over Pr- and Cu-Doped CeO2 Catalysts: Effect of Oxygen Vacancies," *J Phys Chem C* 112 (2008) 15045-15051.

[131] H. K. Lin, H. C. Chiu, H. C. Tsai, S. H. Chien, C. B. Wang, "Synthesis, characterization and catalytic oxidation of carbon monoxide over cobalt oxide," *Catal lett* 88 (2003) 169-174.

[132] W. Liu, T. Deng, L. Feng, A. Xie, J. Zhang, S. Wang, X. Liu, Y. Yang, J. Guo, "Designed synthesis and formation mechanism of CeO2 hollow nanospheres and their facile functionalization with Au nanoparticles," *CrystEngComm* 17 (2015) 4850.

APPENDIX A

EXPERIMENTAL DETAILS

A. 1 Synthesis of Ceria Particles

With the aim of synthesizing ceria nanospheres catalysts, several different methods with different experimental tools were used. First, the microwave-assisted hydrothermal method was used to synthesize ceria hollow nanospheres [104]. Cerium nitrate hexahydrate ($Ce(NO_3)_3 \cdot 6H_2O$, Alfa Aesar), urea (NH_2CONH_2, J. T. Baker) and deionized water were used as precursor materials. 0.5 mmol of cerium nitrate hexahydrate and 0.75 mmol urea were dissolved in 50 mL of deionized water, and the solution was poured into a Teflon-lined autoclave (Parr Microwave Acid Digestion Vessels). The autoclave was tightened and placed in a microwave oven (Panasonic Microwave Oven). The solution was targeted to be heated at 170 °C for 2 minutes by microwave irradiation and placed in the oven until it cools down and reaches room temperature. Then, the solution was collected using a centrifuge and washed with deionized water and ethanol three times in sequence. Finally, the sample was dried at 60 °C for 12 hours and collected.

Figure 35. Microwave oven and Teflon-lined autoclave.

To synthesize ceria nanospheres, the one-step solvothermal method was used and ceria nanospheres were successfully synthesized with an average diameter of around 200 nm with high surface area [132]. 1.25g cerium nitrate hexahydrate ($Ce(NO_3)_3 \cdot 6H_2O$, Alfa Aesar) and 0.5g polyvinylpyrrolidone (PVP K30, Alfa Aesar) were dissolved in 37.5 mL ethylene glycol and 2.5 ml deionized water with 30 minutes of stirring. The transparent solution was poured into a Teflon-lined autoclave of 100 ml capacity and heated for 3 hours at 160 °C in a furnace. After 3 hours, the autoclave was cooled down in the air to reach room temperature. Then, the solution was collected using a centrifuge and washed with deionized water and ethanol three times in sequence. Finally, the sample was dried at 60 °C for 12 hours and collected.

Figure 36. Furnace and Teflon-lined autoclave.

Appendix B

RESULTS AND DISCUSSIONS

B. 1 Ceria Particles

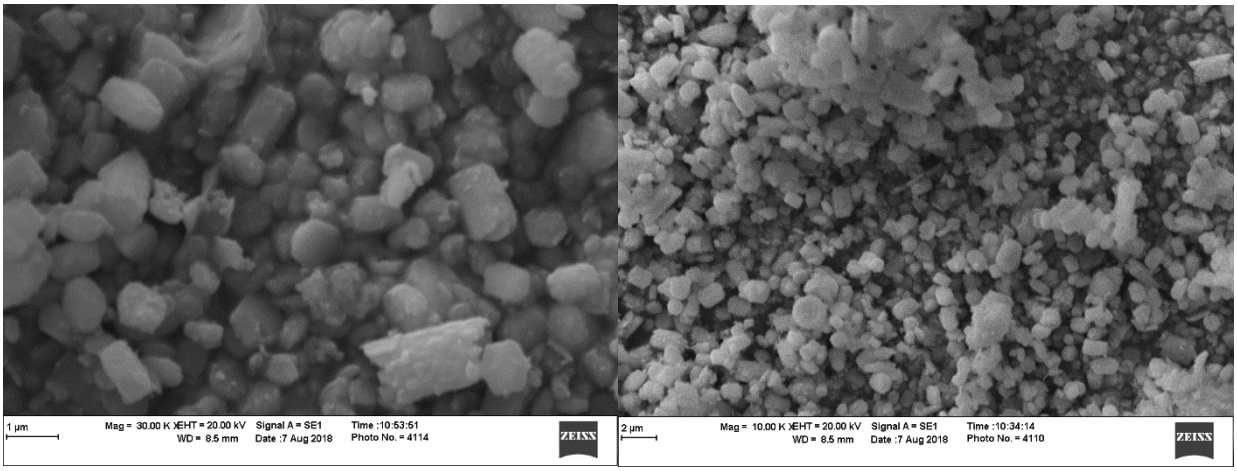

Figure 37. SEM images of ceria particles synthesized using the microwave-assisted hydrothermal method.

Using the microwave oven and autoclave from figure 35, ceria particles in figure 37 were synthesized. They were not homogeneous ceria nanospheres that were aimed for, but they were the mixture of various shapes of micro-sized particles. From the synthesis of particles using the microwave-assisted hydrothermal method, the possibility of creating various shapes of particles was found.

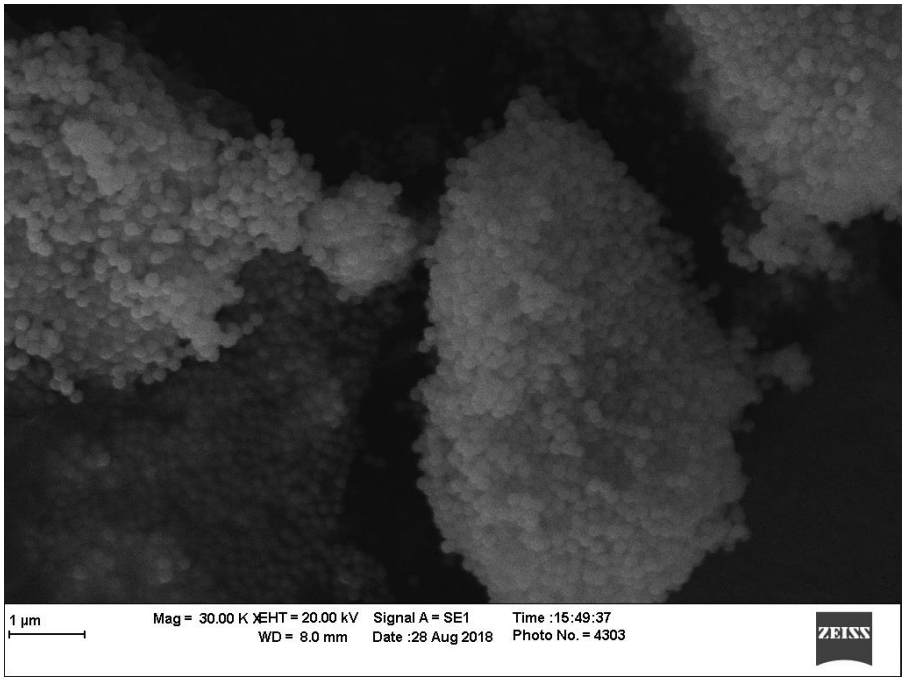

Figure 38. SEM images of ceria nanospheres.

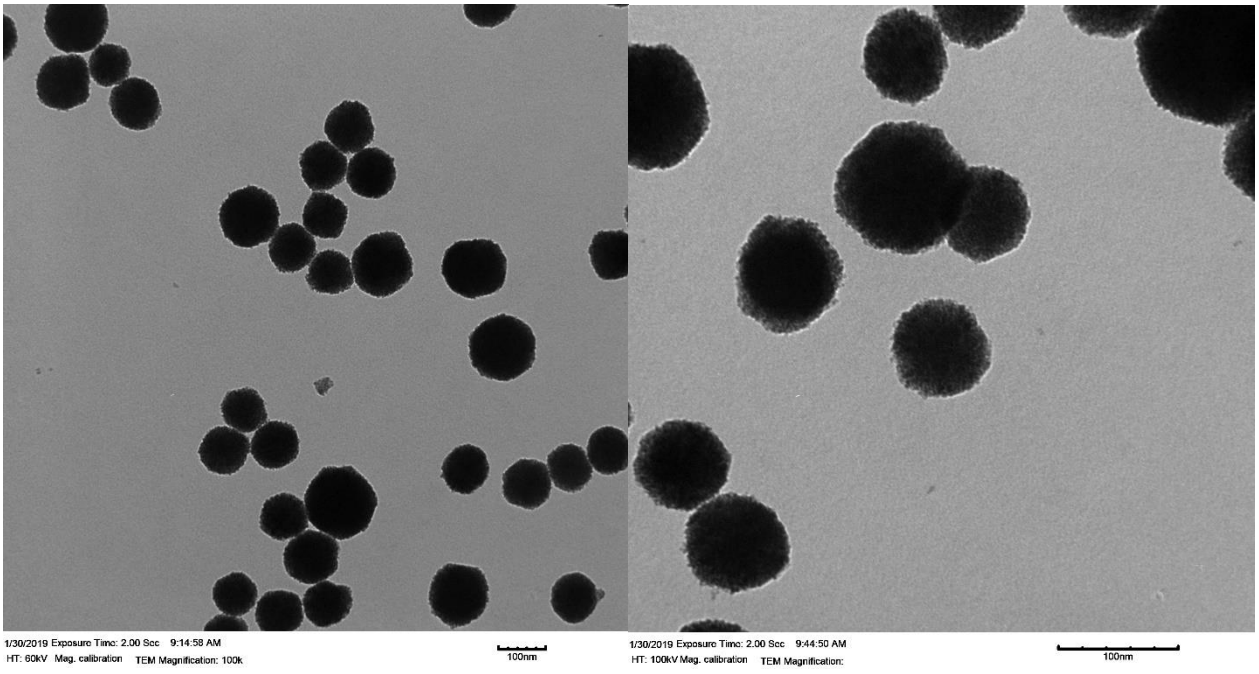

Figure 39. TEM images of ceria nanospheres.

Figures 38 and 39 show the ceria nanospheres synthesized using the one-step solvothermal method. The morphologies of the particles were investigated by SEM and TEM. Ceria nanospheres with an average diameter of around 100 nm were successfully synthesized. The surface area of the sample was measured using the BET machine and it was around 80 m^2/g. To evaluate the catalytic property of the particles, they were used for the CO oxidation experiment. The 0.2g of the sample was used as a catalyst to measure CO oxidation and the result is given below.

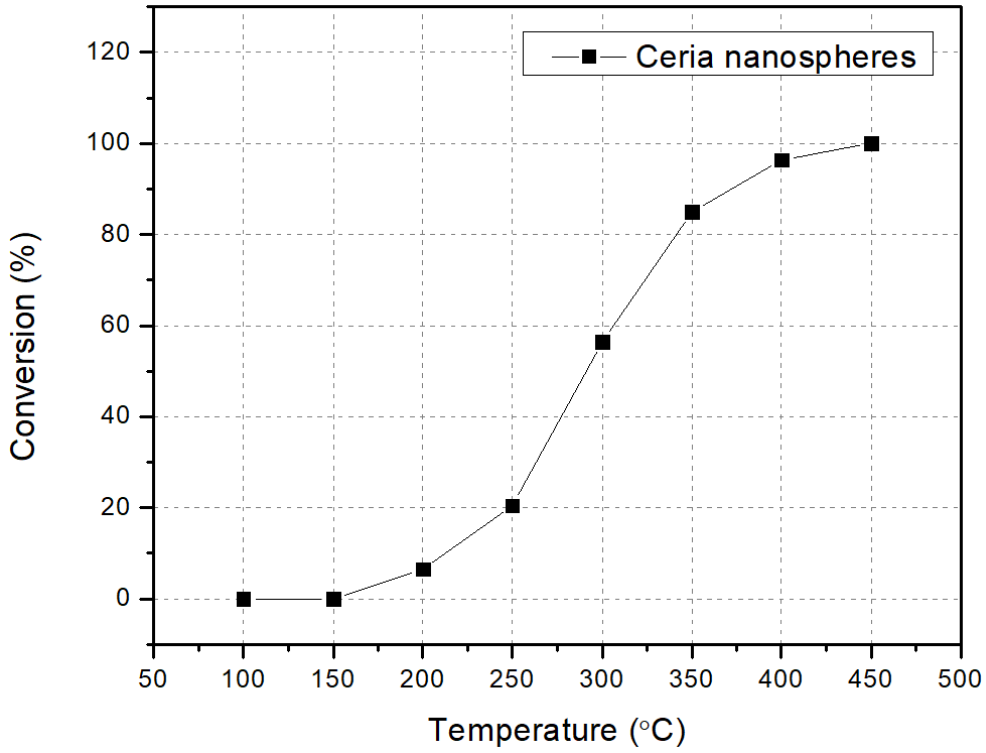

Figure 40. A CO oxidation graph of ceria nanospheres.

Figure 40 shows the CO oxidation graph, and the reaction started conversing CO to CO_2 from the temperature around 200 °C and the reaction reached the 100% conversion at the temperature around 450 °C